metals

Review

Recent Developments in Laser Welding of Aluminum Alloys to Steel

Daniel Wallerstein [1] , **Antti Salminen** [2] , **Fernando Lusquiños** [1], **Rafael Comesaña** [3], **Jesús del Val García** [1], **Antonio Riveiro Rodríguez** [3,*] , **Aida Badaoui** [3] **and Juan Pou** [1]

1   LaserON Research Group, CINTECX, School of Engineering, University of Vigo, Lagoas-Marcosende, E-36310 Vigo, Spain; dwallerstein@uvigo.es (D.W.); flusqui@uvigo.es (F.L.); jesusdv@uvigo.es (J.d.V.G.); jpou@uvigo.es (J.P.)
2   Department of Mechanical and Materials Engineering, University of Turku, FI-20014 Turku, Finland; antti.salminen@utu.fi
3   Materials Engineering, Applied Mechanics and Construction Department, University of Vigo, EEI, Lagoas-Marcosende, E-36310 Vigo, Spain; racomesana@uvigo.es (R.C.); aida@uvigo.es (A.B.)
*   Correspondence: ariveiro@uvigo.es

Abstract: The development of high-performance dissimilar aluminum–steel joints is necessary to promote the feasibility of multi-material design and lightweight manufacturing. However, joining aluminum to steel is a challenging task mainly due to the formation of brittle intermetallic compounds (IMC) at the joint interface. Laser welding is considered a very promising joining process for dissimilar materials, although its application in industry is still limited by the insufficient mechanical performance of the joints. The present paper aims to give a comprehensive review of relevant recent research work on laser joining of aluminum to steel, contributing to highlighting the latest achievements that could boost acceptance of laser joining of dissimilar materials by the modern industries. To this end, the most important challenges in laser joining of aluminum to steel are presented, followed by recent approaches to overcome these challenges, the state-of-art of comprehension of IMC formation and growth, and the different strategies to minimize them.

1. Introduction

Environmental issues have risen the modern industries' concerns on reducing human carbon footprint. Rissman et al. [1] stated that in 2014 industry was responsible for about one-third of global anthropogenic greenhouse gases (GHG) emissions, and they suggested improving the material efficiency as a strategy toward decarbonization of global industry. Lightweighting is considered an important strategy towards material efficiency [2,3], potentially leading to important reductions in GHG emissions [4].

Multi-material design has recently received much attention as a way to reduce weight, improving the performance of technical products and limiting costs [5]. This design concept brings improvements in overall product efficiency, as it permits applying the most suitable material for each component according to the requirements [6]. In order to help multi-material design along, it is necessary to develop technologies for joining dissimilar materials.

Steels and aluminum alloys are, incomparably, the most important metals in engineering applications, being used extensively in construction, transport industry, and industrial equipment [7]. Steels are attractive mainly due to their relatively low price, high strength, toughness, ductility, good weldability and exceptional flexibility of properties as a result of microstructural modifications [8,9]. In turn, aluminum alloys combine light weight, good formability, excellent thermal and electrical conductivity, high strength-to-weight ratio and corrosion resistance [10].

Therefore, dissimilar aluminum–steel joints promote a striking opportunity to achieve smart assemblies, combining interesting properties of both materials and resulting in important weight reduction [11]. However, joining aluminum to steel is considered a very difficult task [12], as inevitable intermetallic compounds (IMC) are formed during the joining process, compromising the integrity of the dissimilar joints.

Due to the important role the IMC layer plays in the mechanical properties of dissimilar joints, most of the research efforts have been focused on controlling IMC formation and growth. It is well known that IMC growth is a diffusion-driven mechanism [13,14], in which the diffusion times [15] and peak temperatures [16] are determinants. Thus, low-heat input welding processes facilitate controlling the formation and growth of the IMC layer, leading to better mechanical performance. In this context, laser welding stands out as a very precise technique [17,18], which enables accurate control of heat input [19] and high cooling rates due to its very high energy density [20].

Joining processes that involve melting such as electron beam welding (EBW) and brazing; and solid-state processes such as friction stir welding (FSW), friction welding (FRW) and explosion welding (EXW) can also be used to join aluminum to steel. EBW is a high-energy-density and very precise welding process [21] and has been successfully used to obtain dissimilar aluminum–steel joints [22]. However, EBW requires a vacuum environment, which is not necessary for LBW [23]. Brazing is a low temperature-joining process that avoids melting the base materials and is suitable for many combinations of dissimilar materials [24]. However, the strength of brazed joints is usually limited [25], hampering its use for structural applications. FSW is a solid-state joining process that uses a non-consumable tool to join the materials, avoiding metallurgical issues present in fusion welding [26], and has been extensively used to join aluminum to steel [27] with excellent mechanical properties [28]. Nevertheless, compared to FSW, laser welding can be applied to weld much more complex geometries [26] and provides much higher productivity [29]. Similarly, in FRW the materials are joined by direct friction without a tool [30]. Although FRW can be used to join dissimilar materials, several issues can arise if the melting characteristics and mechanical properties of the materials differ significantly [31], which is the case of aluminum–steel combination. Additionally, the size of the pieces to be joined is limited by the possibility of mounting them on the available FRW system [31]. Finally, EXW has also been successfully used to join aluminum to steel [32,33], although the technique is limited to simple weld geometries and shows some disadvantages such as high levels of noise and vibration, restricting its applications [34]. Obviously, each technique has its own advantages and limitations, but among the available options to join aluminum to steel, laser welding is definitely a very competitive technique [35].

The present paper aims to review the most relevant recent publications on dissimilar laser joining of aluminum to steel, giving a broad outline of what has been done in this research field, and then discussing in detail the strategies used and the results obtained so far. Therefore, we hope we will further contribute to complement other short reviews already available such as [36] and the recently published [37]. To this end, firstly the main challenges in laser joining of aluminum to steel are presented. Then, the recent approaches to overcome these challenges and obtain sound dissimilar joints are disclosed. Next, the microstructural features of IMCs within dissimilar aluminum–steel joints are shown, followed by discussion, conclusions and future prospects.

2. Challenges in Laser Joining of Aluminum to Steel

Despite the advantages of dissimilar aluminum–steel joints, joining them is a very difficult task. Welding of aluminum alloys is itself challenging owing to the physical properties of these alloys, such as high thermal conductivity, high thermal expansion coefficients, and low viscosity [38]. Moreover, the difficulties in joining aluminum to steel increase substantially. Firstly, this due to the important differences between the physical properties of these two families of materials, which increase the complexity of the joining process [11]. Further, it is also due to the inevitable formation of brittle intermetallics

at the joint interfaces, which can severely deteriorate the mechanical performance of the joints [39].

In fusion welding, some physical properties of the materials being welded are determinant to the process features. Melting range (the range of temperatures through which an alloy transforms completely from solid to liquid state), thermal conductivity and thermal expansion coefficients are examples of thermophysical properties that play a major role in the welding process. For instance, the melting range of materials being fusion welded dictates the energy required in the joining process [40], and obviously, physical phenomena such as melting and solidification, aside from indirectly affecting phase transformations during cooling. Thermal conductivity of materials significantly influences the cooling rates, which in turn determine the final welding microstructures [20]. Moreover, high thermally conductive materials usually need more energy to be welded [41] and present large heat affected zones [42], while low conductive materials are more susceptible to thermal distortions [43]. High thermal expansion coefficients are directly correlated to welding distortion [40,44], and the dissimilar joining of materials having considerably different coefficients results in high level of residual stress [45]. Table 1 collects the above-mentioned thermophysical properties for pure Al and Fe, and for some common aluminum and iron alloys.

Table 1. Thermophysical properties of selected Al and Fe alloys ([46,47]).

Material	Melting Range at Atmospheric Pressure (°C)	Thermal Conductivity Near Room Temperature (W/m K)	Thermal Expansion Coefficient (10^{-6}/K)
Pure Al	660	247	22.8
1100-H18 aluminum alloy	643–655	218	23.6
2024-T3 aluminum alloy	500–638	121	23.2
6061-T6 aluminum alloy	580–650	167	23.6
7075-T6 aluminum alloy	475–635	130	23.6
Pure Fe	1538	80.4	11.7
SAE 1020 carbon steel	1470–1530	46	12
AISI 304 stainless steel	1390–1450	16	17

From the data presented in Table 1, one can notice the significant differences between properties of aluminum alloys and steels: melting temperatures of aluminum alloys and steels differ about 1000 °C from each other, thermal conductivity of aluminum is roughly three times higher than that of iron, and thermal expansion coefficient of aluminum is roughly twice higher than that of iron. Thus, it is not surprising that joining materials belonging to such different families is a challenging task.

Besides all the differences in physical properties, there is another major issue when joining aluminum to steel: the almost zero solubility of iron in aluminum, which is responsible for the formation of intermetallic compounds within the welding zone [36]. Although the formation of IMC is necessary for the effective connection between aluminum and steel [48], the excessive amount of IMC can severely compromise the structural integrity of the dissimilar joints due to their high hardness and brittle behavior [15].

According to Agudo et al. [48], Fe-Al IMCs formation and growth are results of both interdiffusion and chemical reactions between Fe and Al. Therefore, the strategies to control IMC formation and growth have been based on controlling the thermal cycles to which the joints are submitted in order to indirectly control diffusion rates (by applying modified beam shapes, beam oscillation, enhanced heat extraction, etc.), and on chemical composition changes (for instance, studying the influence of different filler metals and/or

fluxes, and welding dilution). These strategies will be shown and discussed throughout the following sections.

Indeed, as IMC formation and growth strongly depend on diffusion rates, it has become a common approach to generate welding-brazing joints, in which the aluminum is melted and the steel remains solid during the process. The reason behind this strategy is that the diffusion rate between solid steel and molten aluminum is much lower than the diffusion rate when both materials are in a liquid state [49], resulting in much slower intermetallic formation rates [50].

3. Approaches to Laser Joining Aluminum to Steel

The most common joints for laser welding are lap, butt, fillet and flange joints [51]; in lightweight design, however, lap and butt joints are the most frequently used, as fillet joints are more common to thick plates and flange joints are applied to pipelines. Lap joints have the inconvenience of increasing both overall weight, due to the overlapping material, and crevice corrosion-related issues [52], due to the presence of small gaps. However, they provide larger mounting tolerances and are easily clamped [53]. Butt joints, on the other hand, are attractive to lightweight design as they have no overlapping material and generally result in higher strength due to complete penetration. However, joint preparation and fit-up might be concerning. Moreover, lap joints are generally autogenous, while butt joints are usually fed with filler metal, which enables controlling the chemical composition of the joints at the expense of potentially increasing weight.

The approaches to obtain dissimilar joints are divided into lap and butt joints, and are presented in the following subsections. The analysis of literature to write this section was made by manually consulting the Scopus and Web of Science databases. The keywords "laser", "joining", "welding", "brazing", "dissimilar", "aluminum" and "steel" were the starting point for the research, which was done several times during the study in order to guarantee that the review is updated with the most recent and relevant publications. A thorough selection of publications was carried out, ensuring that only publications dealing with laser joining of aluminum alloys to steel were included. Priority was given to recent (last 5 years) publications, although some less recent works were also included, as we considered them indispensable to the review. The most important issues in the research field were then identified, and further analysis of the available data was carried out aiming at selecting the publications that dealt with these selected issues. At this point, some crossed references were also consulted and added to our review, although they may not appear in the formerly consulted databases. Finally, we decided to divide the joining approaches into lap and butt joints, and into these two groups, we present the research works grouped, to the possible extent, regarding similitudes in their joining strategies. The authors would like to highlight that the PRISMA 2020 guideline for reporting systematic reviews [54] was followed during this research work.

3.1. Lap Joints

When lap joining aluminum to steel, the first choice one has to take is whether to place aluminum or steel on top. Sierra et al. [39] joined DC04 steel to 6056 and to 6016 aluminum alloys, with no filler metal. They compared the aluminum-on-top to the steel-on-top configuration, and verified that the former is very susceptible to cracking, which they associated with the high crack sensitivity of the studied aluminum alloys. On the other hand, they achieved imperfections-free joints by limiting the penetration depth up to 500 μm in the steel-on-top configuration. In this condition, they observed a 5 to 20 μm-thick IMC layer containing Fe_2Al_5 and $FeAl_3$. It is important to highlight that despite the results found by Sierra et al. [39], both steel- and aluminum-on-top configurations have been successfully carried out by several authors, as it will be shown throughout this subsection.

A clear advantage of the lap joint configuration in dissimilar welding is the high contact area between the dissimilar materials. Additionally, the wettability of molten aluminum on solid steel strongly influences the mechanical performance of the joints. There-

fore, different strategies have been proposed to improve wettability. Xia et al. [55] compared four different shielding gas conditions (pure Ar, 80%Ar-20%CO_2, 50%Ar-50%CO_2, and pure CO_2) to join AA6061 to CR340 cold-rolled steel, and observed an improvement in wettability when CO_2 content increases, although the most important improvement was noticed from pure Ar to 80%Ar-20%CO_2. This improvement was related to the thermal cycles to which the joints were submitted: the higher the CO_2 content, the higher the peak temperature within the weld pool. On the other hand, IMC layer thickness and components changed with higher CO_2 contents: while only $Fe_{1.8}Al_{7.2}Si$ was found in the pure Ar condition, $Fe_2(Al,Si)_5$ and $Fe(Al,Si)_3$ were formed when CO_2 was present. Best mechanical performance was obtained in the 50%Ar-50%CO_2 condition, when a balance between wettability and microstructure was achieved.

Peyre et al. [56] studied joining DC04 low-carbon steel to 6016 aluminum alloy without filler metal. The authors melted the aluminum, which was placed on top, to obtain a fillet weld. They found a 2 to 10 μm-thick IMC layer mainly composed of Fe_2Al_5, and stated that locally thicker IMC layers are prone to cracking. The authors also studied the influence of using zinc-coated steel: they reported an improvement in aluminum wettability in this condition, which they associated with the molten aluminum being spread onto liquid zinc. On the other hand, they reported some issues related to this condition, such as susceptibility to porosity formation due to zinc evaporation, and an increase of crack sensitivity due to the formation of low melting point Al-Zn phases.

Zinc has a much higher equilibrium vapor pressure than aluminum [57], so when the former element is present whether in galvanized steel or in the aluminum alloy as an alloying element, selective evaporation can occur, leading to porosity formation. Thus, several attempts have been made to control zinc evaporation in aluminum–steel joining. Zhang et al. [58] reported zinc evaporation in dissimilar joints of galvanized S235 steel to 6061 aluminum alloy with AlSi5 wire as filler metal, detecting a decrease in the concentration of Zn approaching the joining zone. They highlighted that zinc evaporation also compromises the stability of the welding process. For this reason, Weller et al. [59] proposed a closed-loop laser welding control system to join AA6451 to DX56D low-carbon steel. The temperature of the weld pool was assessed continually by a pyrometer, and the laser power was controlled in order to maintain the temperature within defined ranges, guaranteeing the process is carried out in a conduction regime and limiting zinc evaporation.

Aiming at widening the processing windows for joining 22MnB5 high-strength steel to 6061 aluminum alloy, Huang et al. [60] studied varying laser focusing distance (and consequently laser spot diameter). The authors built a processing map (laser power versus laser spot diameter), defining insufficient wire melting and burn through, respectively, as lower and upper limits for sound weld formation. Although they obtained wider parameter windows for higher laser spot diameter, the average IMC layer thickness in this condition was also higher due to the higher overall heat input (despite the lower energy density). Finally, they found the best mechanical performance for intermediate levels of laser power and spot diameter, in which a compromise between wettability and microstructure was reached. Laser power and spot diameter were also studied by Seffer et al. [61,62] and Lahdo et al. [63]. In these works, linear energy density was considered, and its influence on weld geometry and microstructures was studied. It has been shown that although penetration depth and weld width increase with the energy density, the IMC layer can thicken too much, in such a way that the balance point has to be found in each particular application.

Due to the previously mentioned high thermal expansion coefficients presented by aluminum alloys, distortion is an important concern when welding these alloys. Therefore, several authors proposed special clamping devices to improve their results when welding aluminum to steel. Meco et al. [64] joined AA5083 to XF350 high strength low alloy (HSLA) steel in lap joint configuration. They developed a special clamping device to guarantee the absence of a macroscopic gap between the steel (positioned on top) and the aluminum sheets, improving the thermal contact. Taking advantage of the large difference between aluminum and steel melting temperatures, they promoted the melting of the top surface

of the steel and, by heat conduction, the bottom surface of steel reached temperatures below the melting temperature of steel but above the melting temperature of aluminum. The joining approach and the resulting welding–brazing joint are schematically shown in Figure 1.
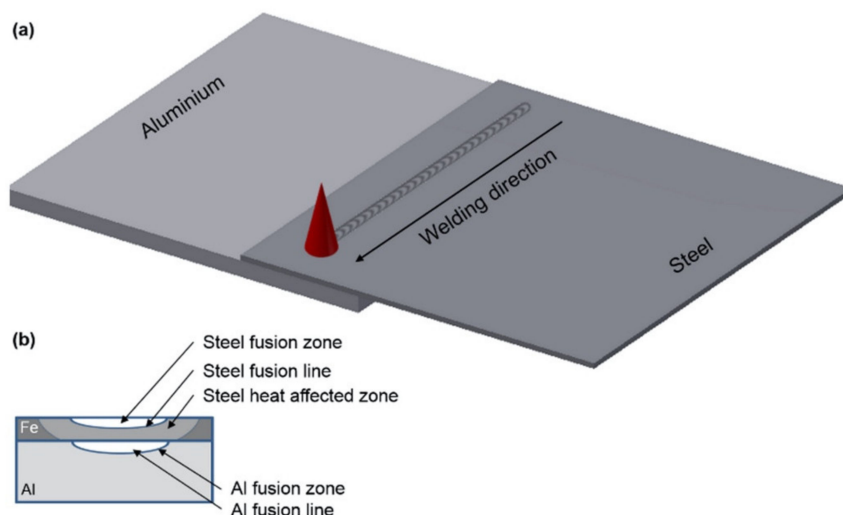

Figure 1. Joining configuration used by Meco et al. (**a**) Overview; (**b**) Resulting welding–brazing joint (schematic). (Reprinted with permission from ref. [20]. Copyright 2017 Elsevier, under the terms of the Creative Commons CC-BY license).

Later, using the same materials and joint configuration, Meco et al. [20] showed that lap joint strength strongly depends on the bonding area. Thus, they proposed a model to predict the aluminum weld width (which defines the bonding area) and the temperature profile within the joints (which strongly influences IMC formation and growth) as a function of laser parameters. The best strength was obtained when the bonding area was maximized and IMC layer thickness was minimized.

In order to improve the thermal contact between the pieces to be joined, a special clamping device was also developed by Liedl et al. [19] to lap-join 6016 aluminum alloy to DC01 low-carbon steel. Additionally, the authors used different backing block materials (aluminum, steel and copper) to control the heat extraction from the joining zone, besides a water-cooled backing block to further improve heat extraction. However, the heat extraction provided by the water-cooled backing block was so high that it impeded the formation of a sound joint, and the authors concluded that the copper backing block led to the best results. Indeed, copper backing blocks have been commonly considered an interesting choice, as highlighted by Guan et al. [65].

Also interested in providing enhanced thermal contact between the dissimilar sheets, Fan et al. [66] used a pressing roller-assisted laser welding system to join 99.5% pure aluminum to DC01 steel. The authors reported that although peak temperature, cooling time and integral of the thermal cycle (the area below the temperature–time curve during welding) increased linearly with laser power, the IMC layer thickness increased in a non-linear way: for low laser powers, the thickness increased rapidly, while for high laser powers it seemed to go towards an asymptote. They also found similar behaviors regarding the dependency of IMC layer thickness on peak temperature, cooling time and integral of thermal cycle, observing faster increases at the beginning of the curves than at the end. Finally, they stated that the cooling time exerts the strongest influence on the IMC layer thickness among the studied thermal factors.

The importance of IMC formation and growth to the mechanical properties of dissimilar joints has already been presented. Therefore, several authors proposed modifications of beam profiles in order to achieve better control of the welding thermal cycles, resulting in limited IMC layer thickness.

Yan et al. [67] joined AA6111 to JSC270CC structural steel using a dual-beam configuration composed of a continuous-wave (CW) beam and a pulsed-wave (PW) one. The configuration is shown in Figure 2.
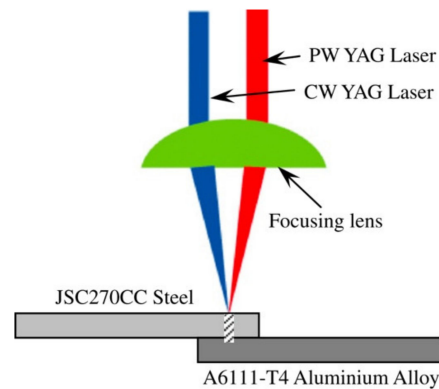

Figure 2. Dual-beam configuration, combining a pulse-wave (PW) and a continuous wave (CW) beam, proposed by Yan et al. (Reprinted with permission from ref. [67]. Copyright 2010 Elsevier).

The authors claimed that the pulsed beam was responsible for a resulting root-shaped IMC layer free of imperfections, which improved the mechanical resistance of the joints. Likewise, the resulting IMC layer was much thinner (almost one order of magnitude) than the one formed when only CW beam is applied.

Cui et al. [68] used an in-line dual-beam configuration to join AA6061 to Q235 carbon steel, shown in Figure 3. In the proposed configuration, the power was distributed unevenly between the two beams, giving rise to the main and secondary beams shown in Figure 3.
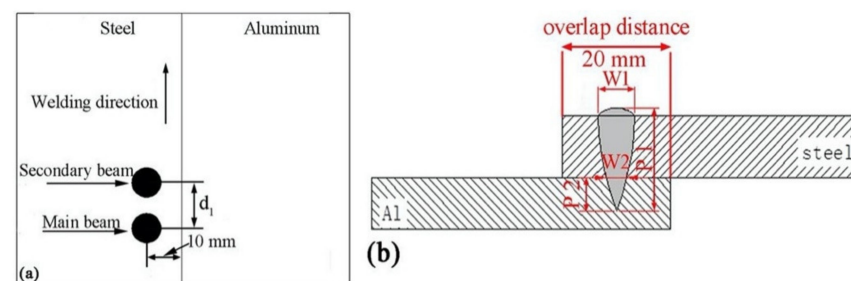

Figure 3. In-line dual-beam configuration used by Cui et al. [68]. (**a**) Top view; (**b**) Cross-sectional view. dl is the distance between main and secondary beams, W1 and W2 are, respectively, the top weld width and weld width at the interface, P1 and P2 are, respectively, total penetration depth and penetration depth within the aluminum sheet. Reprinted with permission from ref. [68]. 2018 Elsevier.

The influence of power distribution and distance between main (trailing) and secondary beam (leading) were assessed. The authors found the best mechanical results when the power ratio between the secondary beam and main beam was 0.67 and the distance between beams was 1.5 mm. The good mechanical behavior was attributed to the absence of welding imperfections, to an adequate weld shape represented by a high depth to width ratio, and to a mixed failure pattern with some plastic deformation.

Aiming at improving the wettability of aluminum on steel, Yuan et al. [69] also investigated a dual-beam configuration, which consisted of a lap joint with aluminum on top and no filler metal. In their study, 20% of total laser power was used in a derived beam directed onto the steel sheet, while 80% of laser power was maintained in the main beam positioned on the aluminum sheet. Figure 4 illustrates the joining configuration.
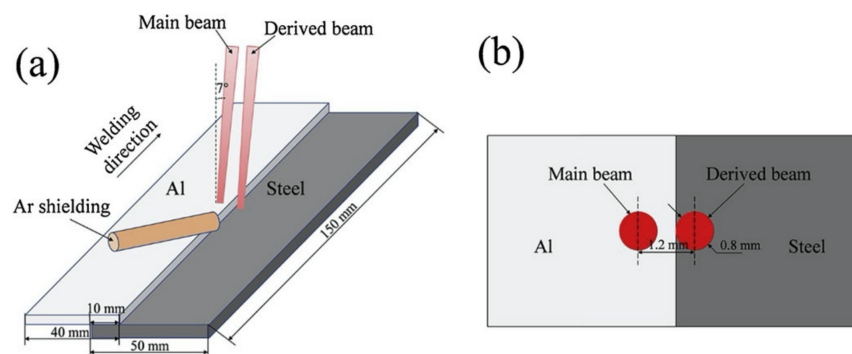
Figure 4. Dual-beam joining configuration used by Yuan et al. (**a**) Overview; (**b**) Top view. (Reprinted with permission from ref. [69]. Copyright 2019 Elsevier).

The authors observed an improvement of wettability with higher laser power at the expense of the formation of a thicker IMC layer, and stated that an intermediate laser power led to the best mechanical results providing a balance between wettability and IMC thickness.

In spite of the advantages of avoiding melting the steel, Su et al. [70] proposed a different strategy to join AA5052 to galvanized Q235 steel in lap joint configuration using a single beam: instead of pointing the laser at the surface of the upper plate, as usual, the authors positioned the aluminum sheet on top, pointed the laser spot at the intersection between the sheets, and fed a Zn-based wire to obtain a fillet weld along the contact edge. As both the aluminum and the steel sheets were melted, the authors defined two fusion zones (FZs) within the joints, the first one being composed of filler metal and molten aluminum, and the second one corresponding to the molten steel. Yang et al. [71] also proposed a single-beam approach with improved energy distribution, based on beam oscillation. The processing parameter window was enlarged with increased oscillation amplitude, which also improved the homogeneity of temperature distribution and consequently of IMC layer thickness.

Another option to redistribute the energy applied to the materials is to modify the beam profile instead of dividing the beam: Indhu et al. [72] used a diode laser with a top-hat beam profile (instead of the standard Gaussian beam profile) to join DP600 dual-phase steel to 6061 aluminum alloy. The authors proposed controlling power density and interaction time in order to obtain good weld penetration and desired microstructure, composed of a thin IMC layer. Additionally, they sought for a reduced heat-affected zone (HAZ), as steel HAZ softening is an important issue when applying dissimilar welds to tailored blanks.

Beyond modifying the beam shape, another way to control the welding thermal cycles is by modifying the laser wave characteristics. Torkamany et al. [73] used a pulsed laser beam to join AA5754 to low-carbon steel without filler metal, positioning the steel on top. Firstly, the authors varied peak power and pulse duration in such a way that pulse energy and mean power were kept constant. They found that high peak power, which resulted in beads showing high depth to width ratio and high amount of IMCs, was responsible for high levels of imperfections such as porosity and cracks, and for high Al content within the steel due to upward movement of aluminum. They stated that IMCs not only show high hardness and brittleness, but also have different thermal expansion coefficients both from aluminum and steel, promoting crack propagation. Next, they varied pulse duration and mean power, maintaining constant all other parameters including peak power. They found that high pulse duration increased penetration depth, bead width and amount of IMCs. Lastly, they studied the influence of overlapping factors (intersection area impinged by two successive pulses) on joints' characteristics by varying welding speed and maintaining all other parameters constant. They stated that a minimum overlapping factor is necessary in order to avoid insufficient bonding and important porosity formation. On the other hand, too high overlapping factors led to excessive IMC formation, compromising joint strength. After all these analyses, the authors concluded the study defining the parameters

combination that led to the best mechanical performance. Pulsed laser welding was also studied by Pereira et al. [74] to join AA1050 to DP1000 steel. The authors assessed the application of different laser powers, pulse durations, overlapping factors, laser spot diameters and welding speeds and found a combination of parameters that led to sound joints showing satisfactory mechanical performance, and highlighted the importance of correctly choosing the processing conditions. Adjusting the processing parameters in order to optimize mechanical performance was a concern also for Liu et al. [75]. In their study, the authors varied laser power, welding speed and laser defocusing, aiming at finding the heat input that provided the balance between effective connection and IMC formation.

Although lap joints are commonly welded autogenously, filler metals can be used in order to generate beneficial chemical modifications to the weld metal. These chemical modifications can facilitate control of welding imperfections, and improve the microstructures of the welds. Mathieu et al. [76] joined AA6016 to galvanized low-carbon steel in a modified lap joint configuration, using ER4047 (Al-12%Si) wire. The aluminum sheet was bent 90 degrees in order to obtain a fillet-like joint as shown in Figure 5. The filler wire and the laser spot were positioned to coincide at the welding zone. However, while the wire was guided by the geometry of the joint, the laser beam had to be thoroughly aligned.
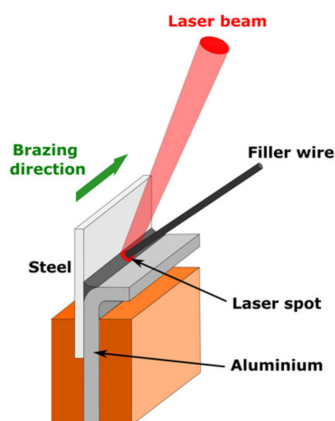

Figure 5. Modified lap joint configuration proposed by Mathieu et al. (Adapted with permission from ref. [76]. Copyright 2006 Elsevier).

The authors stated that in this configuration, the ER4047 wire fed at room temperature did not lead to enough wettability, and found that preheating the wire led to significant improvements in wettability. Finally, the authors highlighted that the tightening torque applied by the welding fixture on the samples influences the wettability and has to be controlled in the process setup.

Later, Mathieu et al. [77] used a Zn-15%Al wire to join the same materials as in [76], but in a slightly different joint configuration (lap joint shown in Figure 6).

Again, the filler wire was fed directly into the weld pool (coincident with the laser spot at the welding axis), in such a way that the laser beam does not impinge on the base materials directly. Besides the single beam configuration shown in Figure 6, the authors also used an in-line dual beam (two beams aligned to the welding direction, also known as tandem configuration) to improve wettability and mechanical performance. They observed a direct relation between brazed seam length (which in turn is related to wettability) and joint strength. Finally, they stated that the seam length per wetting angle ratio is directly proportional to the mechanical strength of the joints.
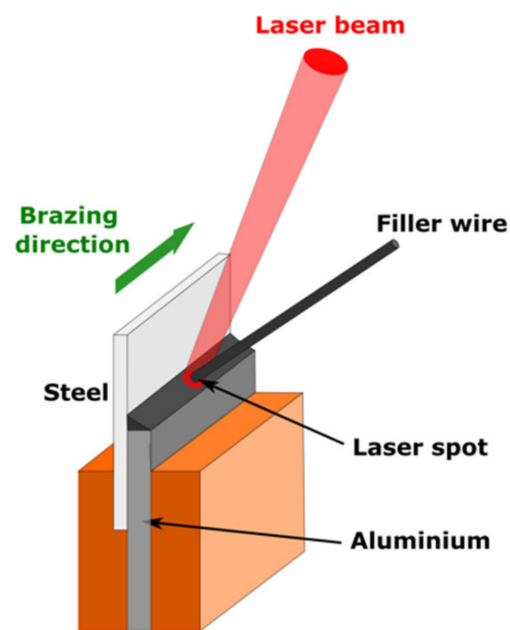
Figure 6. Joint configuration studied by Mathieu et al. (Adapted with permission from ref. [77]. Copyright 2007 Elsevier).

Seeking for controlling porosity formation due to zinc evaporation in dissimilar joints of 5052 aluminum alloy to galvanized SPCC steel, Ogura et al. [78] proposed to insert a 50 μm-thick Ti interlayer between the dissimilar sheets. Although thermal deformation of Ti insert was observed, porosity was significantly suppressed, resulting in much better mechanical performance in comparison to the joints without the Ti insert. Additionally, by varying laser power and welding speed with a constant wire feed speed, the authors defined the processing parameters window that led to sound joints without the occurrence of welding imperfections such as insufficient wire melting or burn through.

Non-conventional filler metals were studied also by Liu et al. [79]: the authors proposed the application of high-entropy powders to inhibit IMC formation and growth in dissimilar joints of 304 stainless steel to 6061 aluminum alloy. By using CoZnCuMn0.8Si0.2 and FeCoCrNiMn high-entropy powders obtained by dry ball milling, they obtained an important decrease in the diffusion of Fe from the welding zone (WZ) toward the unmixed zone (a zone between WZ and HAZ that they observed in all joints in the study). The results were much thinner Fe-Al IMCs in the unmixed zone in comparison to when commercial Al-12%Si powder was used, and the complete absence of IMCs in the WZ. The authors explained that the high-entropy alloys are capable of delaying precipitate nucleation by diffusing and redistributing different elements, resulting in solid solutions or amorphous structures instead of IMCs.

Several authors sought for microstructural improvements and modifications of weld pool dynamics by adding external magnetic fields to the joining system: Chen et al. [80] explained that magnetic fields reduce the diffusion rates of both carbon and aluminum, reducing austenite grain size and IMC layer thickness, respectively. Later, Yan et al. [81] proposed the application of an external magnetic field to assist in joining 6061 aluminum alloy to galvanized DP590 steel in lap joint configuration (see Figure 7). By positioning the steel on top and applying up to 200 mT magnetic flux density, they could improve the control of the joint cross-section (transforming it from cylindric to conic), reducing the element segregation, decreasing the occurrence of cracking, and refining the resulting microstructure.
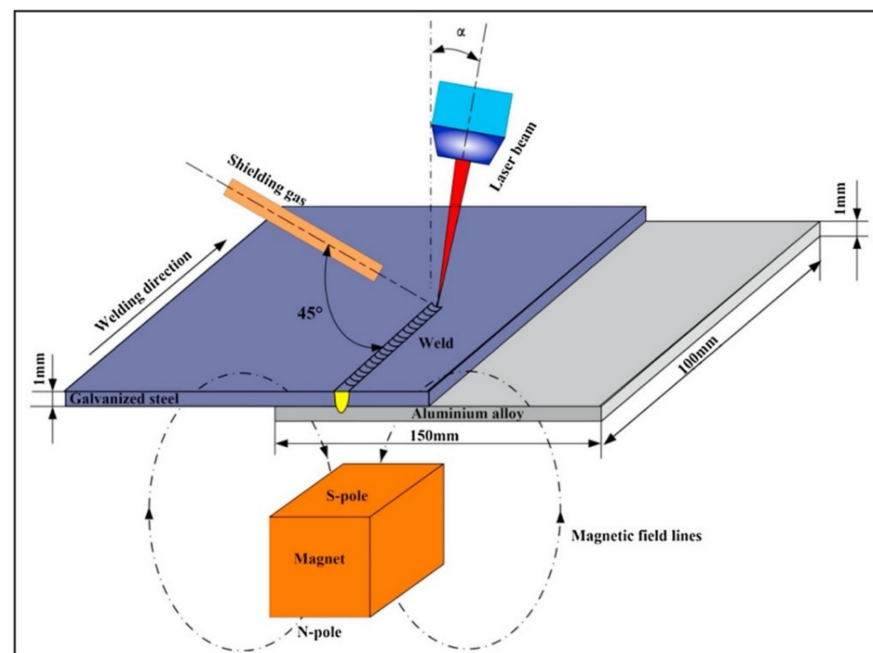
Figure 7. Magnetic field-assisted laser joining configuration proposed by Yan et al. (Reprinted with permission from ref. [81]. Copyright 2019 Elsevier).

More recently, Yan et al. [82] connected coils to an alternating current power supply to study the influence of alternating magnetic fields (50 Hz frequency) on joining AA6061 to galvanized DP590 steel. They managed to enhance the wettability of aluminum on steel and also to reduce IMC layer thickness (although it showed some local heterogeneities), leading to improvements in mechanical performance.

3.2. Butt Joints

Unlike the lap joint configuration, the contact area in butt joints is limited by the thickness of the pieces being joined. Thus, the use of a brazing flux has become very common when joining aluminum to steel in butt configuration in order to improve the wettability of molten aluminum on solid steel [83]. Additionally, it is also a common practice to bevel the workpieces (at least steel side) to obtain a larger contact area, although this additional preparation step increases total operation time and cost. In this sense, Sun et al. [84] joined 60°-beveled AA6061 to 30°- and 45°-beveled zinc-coated low-carbon steel, employing ER4043 welding wire. The authors reported a competitive effect regarding the bevel angle of steel sheets: although the 30° bevel angle in the steel plate resulted in a thicker IMC layer, which leads to worse mechanical behavior due to the brittle characteristic of the IMCs, the resulting bonding area was large enough to compensate for this strength loss. Additionally, they found a heterogeneous IMC layer, and related the heterogeneities to different local thermal cycles: the higher peak temperatures reached by regions closer to the laser heat source led to a locally thicker IMC layer.

Another interesting study of the influence of groove shape on the characteristics of dissimilar joints was carried out by Li et al. [85]. They assessed three combinations of bevel characteristics at aluminum and steel sides, respectively: half-V and square; half-Y and half-Y; and half-Y and half-V. Figure 8 shows the three combinations of groove shapes used by the authors in the study.
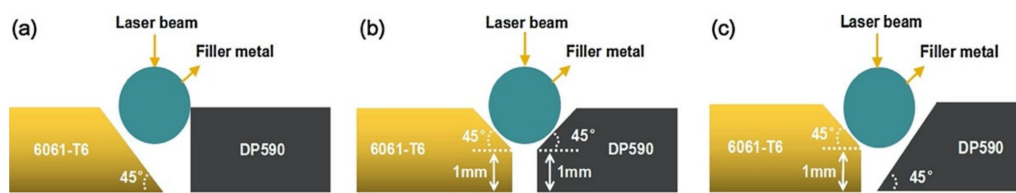
Figure 8. The three different combinations of groove shapes studied by Li et al. Beveling at aluminum and steel, respectively: (**a**) half-V and square; (**b**) half-Y and half-Y; and (**c**) half-Y and half-V. (Reprinted with permission from ref. [85]. Copyright 2018 Elsevier).

The best wettability of aluminum on steel at weld root was obtained when steel was half-V beveled (Figure 8c). Additionally, this condition was responsible for the thinnest and most uniform IMC layer (although thickness decreased from top to bottom). They concluded that the best wettability, the best IMC layer characteristics and the largest bonding area promoted by condition c, were all responsible for the best mechanical behavior under tensile testing.

In another research work, the same authors [86] applied a 45° bevel angle on both aluminum and steel sheets, as well as a 1.0 mm root opening (gap). The joining configuration is shown in Figure 9.
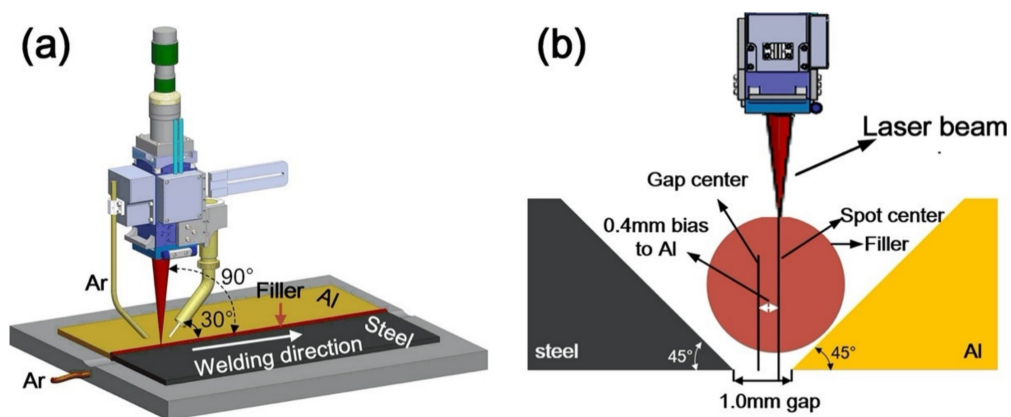

Figure 9. Joining configuration used by Li et al. (**a**) Overview; (**b**) Cross-sectional view. (Reprinted with permission from ref. [86]. Copyright 2018 Elsevier).

The authors adjusted the laser power in order to find the adequate heat input: too low laser power would lead to a lack of fusion, while too high laser power would lead to imperfections such as undercuts and sagging, not to mention that the IMC layer would thicken due to excessively high heat input. Variations in laser power were also responsible for the formation of different IMCs, influencing the mechanical behavior of the joints. The joints that presented the highest resistance under the tensile test were the ones joined at an intermediate laser power of 2200 W. The authors related good mechanical behavior to the absence of welding imperfections, a good wettability of aluminum on steel, and to the formation of a suitable IMC layer.

The use of filler metals is much more common in butt joints than in lap joints. Thus, several authors have studied the influence of different filler metals in order to improve the mechanical properties of dissimilar aluminum–steel butt joints. Xia et al. [87] assessed the application of pure aluminum, Al-5%Si and Al-12%Si welding wires to join non-beveled AA6061 to 45°-beveled DP590 dual-phase steel. They obtained only binary Fe-Al IMCs in the pure Al-wire condition, while ternary Fe-Al-Si IMC were found with the application of Si-containing wires. Although the IMC layer of Al-12%Si wire condition was the thinnest, the authors found the best mechanical behavior in the joints generated with Al-5%Si wire. The authors attributed this result to the formation of a thin IMC layer composed of $Fe(Al,Si)_3$ and $Fe_2(Al,Si)_5$ in the joints welded with Al-5%Si wire, while the Al-12%Si wire

resulted in an IMC composed of Fe(Al,Si)$_3$ and Fe$_8$Al$_2$Si. To support their claim, the authors showed that the fracture under tensile stress was initiated along the Fe$_2$(Al,Si)$_5$ layer in the samples generated with Al-5%Si wire, while in the samples joined with Al-12%Si wire the fracture was initiated at the interface between steel and Fe(Al,Si)$_3$. Moreover, the wettability of molten aluminum on solid steel was much better in the joints generated in Al-5%Si wire conditions compared to those made with Al-12%Si, which could also influence the mechanical performance of the joints.

Besides the more commonly used Al-Si filler metals, several authors have studied other filler metals whether in wire or in powder form. Tan et al. [88] assessed the application of Zn-2%Al, Zn-15%Al and Zn-22%Al flux-cored wires to join 45°-beveled AA6061 to non-beveled DP590 steel. The IMC layer was composed mainly of Fe$_2$Al$_5$Zn$_{0.4}$ layer in all conditions. Additionally, continuous layers of FeZn$_{10}$ were found adjacent to steel when Zn-2%Al and Zn-15%Al were used, and scattered islands of the same phase were detected in all joints. Although the joints welded with Zn-22%Al wire showed the thickest Fe$_2$Al$_5$Zn$_{0.4}$ layer among the three studied conditions, these joints showed the best mechanical behavior, which the authors related to the absence of continuous FeZn$_{10}$ layer. Xia et al. [16] proposed the application of laser powder deposition to join AA6061 to DP590. By depositing two layers of spherical AlSi10Mg powder in a V-grooved butt-joint (shown in Figure 10), they studied the influence of laser power on the joint formation and stated that although high laser power led to a thicker IMC layer, a minimum power was necessary to achieve a reaction layer without which there is no effective bonding.
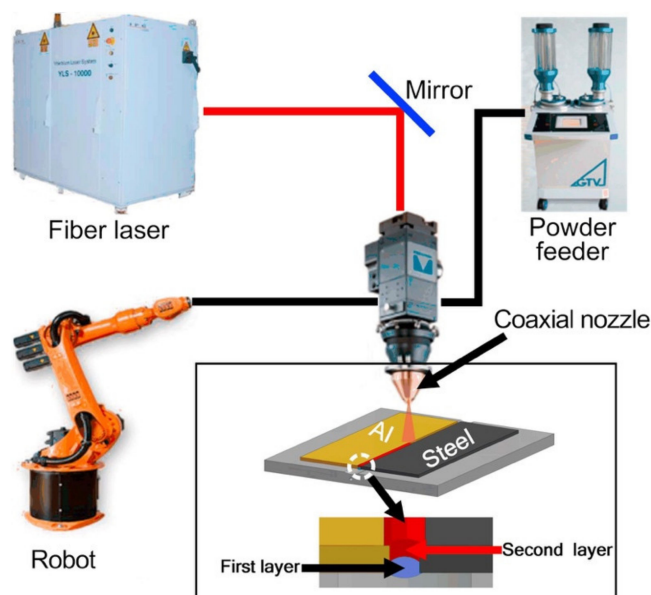

Figure 10. Two layers of laser powder deposition used by Xia et al. to join aluminum to steel in butt joint configuration. (Reprinted with permission from ref. [16]. Copyright 2019 Elsevier).

The authors also claimed that, compared with laser welding with wire feeding, the higher welding speed provided by laser powder deposition led to faster thermal cycles and resulted in the formation of a thinner and more homogeneous IMC layer, improving joint strength. Moreover, the deposition of the second layer of powder could act as heat treatment, leading to fewer residual stresses.

Wallerstein et al. [89] proposed the combination of Al-5%Si welding wire and pre-placed eutectic Al-12%Si powder to join S235 structural steel to AA6061. The joining approach is shown in Figure 11.
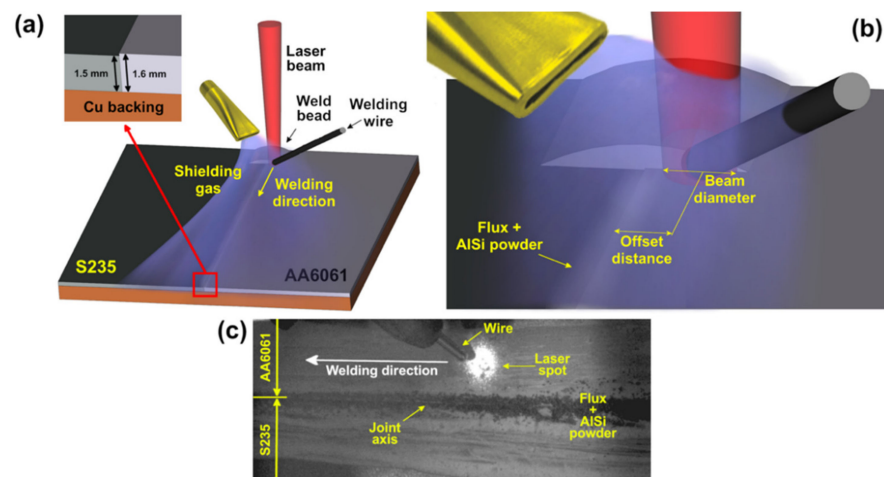
Figure 11. Welding–brazing approach proposed by Wallerstein et al.: 45 degrees-tilted welding wire in combination with preplaced AlSi powder mixed to the brazing flux. (**a**) Overview; (**b**) Detailed processing area; (**c**) Picture of joining setup. (Reprinted with permission from ref. [89]. Copyright 2021 Elsevier).

Sound joints were obtained, whose satisfactory mechanical properties were associated with the good wettability of aluminum on steel due to the 45° degrees inclination of welding wire towards steel, combined with the wettability improvement provided by the preplaced powder, especially at the weld root. Additionally, a combined parameters analysis was carried out in order to elucidate the relation between processing parameters and imperfections formation. The thin and homogeneous IMC layer was composed of Fe_2Al_5, Fe_4Al_{13} and $Fe_4Al_{17.5}Si_{1.5}$.

Modifications of beam profiles applied to lap joints were presented in the previous subsection. Similarly, modified beams have also been applied to butt joints. Xia et al. [90] studied the application of single beam, cross, and in-line dual beams to butt-join AA6061 to DP590 dual-phase steel. Figure 12 shows the configuration used by the authors, in which one can see the three-beam configurations used. Additionally, one can notice that the authors used a thermocouple to assess the thermal cycles during the process.
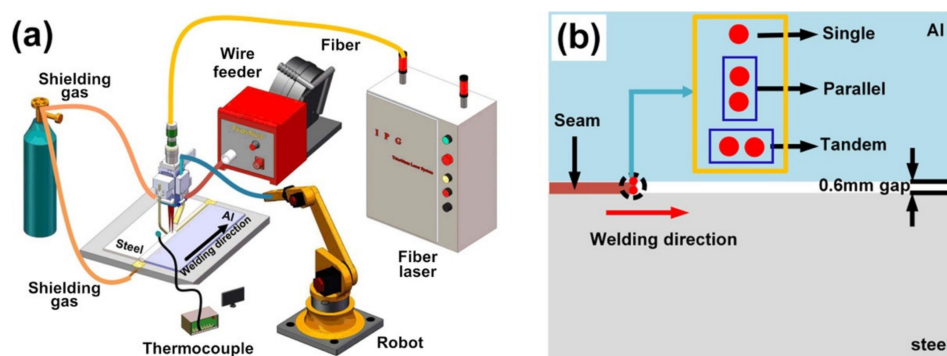
Figure 12. Joining configuration used by Xia et al. (**a**) Overview; (**b**) Top view. (Reprinted with permission from ref. [90]. Copyright 2020 Elsevier).

To improve wettability, the authors used a V-shaped groove (45° bevel angle on both sides) and a 0.6 mm gap distance. Single beam welding resulted in the highest level of porosity and thickest IMC layer, and consequently worst mechanical behavior. In contrast, the application of cross dual laser beam configuration resulted in the formation of the thinnest IMC layer, no porosity, and the best mechanical performance under the tensile test. The authors attributed the best results to the most homogeneous temperature distribution and to the lowest peak temperatures provided by the cross dual beam configuration,

which were demonstrated both by thermocouple measurement and finite element method (FEM) analysis.

Hybrid laser-arc welding (HLAW) combines a laser beam and an arc source in order to produce a synergic welding process and overcome some limitations of the individual processes [91]. Thus, some approaches involving HLAW have also been proposed to join aluminum to steel. Chen et al. [92] used hybrid laser-CMT (Cold Metal Transfer) to join AA5052 to Q235 steel. The authors studied the influence of processing parameters such as wire feed speed, offset distance (distance between the laser spot and the aluminum–steel interface) and welding speed on the characteristics of the resulting joints. In CMT welding the wire feed speed is proportional to the arc current, and consequently also to the heat input. Therefore, the wire feed speed was found to influence porosity formation, shape of the joints, and thickness of the IMC layer. Offset distance, in turn, showed a strong influence on the strength of the joints: too low offset distances led to high IMC layer thickness, resulting in cracking. On the other hand, too high offset distances resulted in low wettability of molten aluminum on solid steel. Finally, a similar effect was shown to take place regarding welding speed: higher welding speeds led to thinner IMC layers, as the heat input is reduced. However, if the welding speed is too high, wettability was compromised.

Laser-CMT was also studied by Meng et al. [93]: they proposed the application of circular beam oscillation to butt-join AA6061 to AISI304 stainless steel, shown in Figure 13.
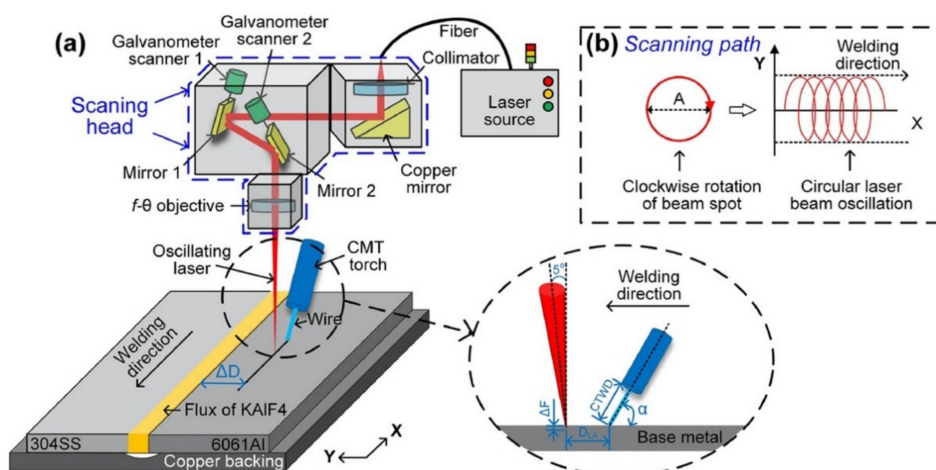

Figure 13. Circular beam path configuration used by Meng et al. (**a**) Overview; (**b**) Top view. ΔD is the laser offset distance, A is the oscillating amplitude, ΔF is the defocusing distance, α is the angle between arc torch and base metal, CTWD stands for "contact tip to workpiece distance", and D_{LA} is the laser-arc distance. (Reprinted with permission from ref. [93]. Copyright 2020 Elsevier).

The authors varied the laser offset distance keeping all other processing parameters constant, and found that the offset distance strongly influences not only the formation of welding imperfections, but also the Fe element distribution within the fusion zone and the characteristics of the IMC layer. The authors stated that an even distribution of Fe led to a homogenous IMC layer, resulting in the best mechanical performance.

It is interesting to notice that, although the attempts to enhance the bonding area of butt joints usually take relatively complex approaches, the mechanical performance of the resulting joints is also usually much better than if direct laser welding without filler metal is applied to this type of joint [94].

Table 2 collects the above-discussed works on laser joining of aluminum to steel recently published. Some useful information regarding materials and methods applied by the authors are summarized, along with some results such as joints' mechanical properties and intermetallic compounds detected.

Table 2. Recent publications on laser joining of aluminum to steel.

Joint Type	Laser System	Aluminum Alloy	Steel	Filler Metal	Joining Approach	Mechanical Properties	Reported IMCs	Ref.
Lap	Continuous Wave (CW) Nd:YAG laser, 3.5 kW max. power	6016 Thickness not reported	Low-carbon steel (0.002% C) Thickness not reported	ER4047 solid wire	Preheated wire	195 N/mm max. tensile resistance	$FeAl_3$, $Fe_3Al_3Si_2$, $Fe_2Al_{7.4}Si$	[76]
	CW Nd:YAG laser, 3.5 kW max. power	6016 Thickness not reported	Low-carbon steel (0.002% C) 0.77 mm-thick	ZnAl15	In-line dual beam	230 N/mm max. tensile resistance	Fe_2Al_5, $FeAl_3$	[77]
	CW Nd:YAG laser, 3 kW max. power	6016 1 mm-thick	DC 04 (both galvanized and non-galvanized) 1.2 mm-thick	None	Aluminum on top, fillet weld	230 MPa max. tensile strength	Fe_2Al_5	[56]
	CW Nd:YAG laser, 3.5 kW max. power	6056 1.3 mm-thick, 6016 1 mm-thick (the authors used a stepped lap joint, the thicknesses refer to the joint location)	DC 04 1.2 mm-thick	None	Both aluminum- and steel-on-top, keyhole regime, control of penetration depth, two parallel beads	250 N/mm max. shear load	Fe_2Al_5, $FeAl_3$	[39]
	Pulsed Wave (PW) Nd:YAG laser, 400 W max. mean power	5754 2 mm-thick	St14 0.8 mm-thick	None	Pulsed laser, steel on top	Approx. 300 MPa max. tensile strength	$FeAl$, $FeAl_2$, $FeAl_3$, Fe_3Al, Fe_2Al_5	[73]
	CW/PW YAG laser, CW: 390 W; PW: 2.61 kW	6111 1.2 mm-thick	JSC270CC 0.8 mm-thick	None	Steel on top, dual beam (one in CW and another in PW)	128 MPa max. shear strength	$FeAl$, Fe_3Al	[67]
	CW lamp-pumped Nd:YAG laser, 4 kW max. power	Al (99.5% purity) 1 mm-thick	DC01 0.75 mm-thick	None	Steel on top, pressing roller to improve heat transfer	Not reported	Not reported	[66]
	CW fiber laser, 8 kW max. power	5083 6 mm-thick	XF350 2 mm-thick	None	Steel on top, special clamping device	30 kN max. shear load	Fe_2Al_5, $FeAl_3$	[20,64]

Table 2. *Cont.*

Joint Type	Laser System	Aluminum Alloy	Steel	Filler Metal	Joining Approach	Mechanical Properties	Reported IMCs	Ref.
	CW disk laser, 5 kW max. power	6451 1 mm-thick	DX56D (galvanized) 0.8 mm-thick	None	Aluminum on top, cross-line dual beam	146 MPa max. tensile strength	FeAl, Fe_2Al_5, $FeAl_3$	[59]
	CW fiber laser, 2 kW max. power	5754 2 mm-thick	301 stainless steel2 mm-thick	None	Steel on top, application of external magnetic field with different intensities keeping laser parameters constant	2.91 kN max. tensile load	Fe_2Al_5, $FeAl_3$	[80]
	CW disk laser, 16 kW max. power	6016 1.15 and 2.0 mm-thick	1 mm-thick HX220LAD high-strength low-alloy steel, 1.25 and 1.50 mm-thick 22MnB5 ultra high strength steel, and 1.0 and 1.50 mm-thick 304 stainless steel	None	Steel on top, assessment of linear energy density	3.50 kN max. tensile load	Not reported	[61]
	CW lamp pumped Nd:YAG, 3 kW max. power	6016 1 mm-thick	DC01 1 mm-thick	None	Aluminum on top, special clamping device, backing blocks (aluminum, steel, cupper, water-cooled)	16 kN (approx..) max. shear load	Not reported	[19]
	CW disk laser, 16 kW max. power	6082 1.5 mm-thick	304 stainless steel 1.5 mm-thick	None	Steel on top, up to 3 welding seams, assessment of linear energy density	6.41 kN max. shear load	Not reported	[62]
	CW fiber laser, 6 kW max. power	6061 1.5 mm-thick	Q235 1.5 mm-thick	None	Steel on top, in-line dual spot laser beam, different energy distribution and distances between beams	115.6 N/mm max. tensile shear resistance	$FeAl_2$, Fe_2Al_5, Fe_4Al_{13}	[68]

Table 2. *Cont.*

Joint Type	Laser System	Aluminum Alloy	Steel	Filler Metal	Joining Approach	Mechanical Properties	Reported IMCs	Ref.
	CW diode laser, 10.4 kW max. power	6082 8 mm-thick	S355 5 mm-thick	None	Steel on top, variation of parameters to assess influence of linear energy density	8 kN max. shear load	Fe_2Al_5, $FeAl_3$, FeAl	[63]
	CW fiber laser, 6 kW max. power	6016 1 mm-thick	DC04 1 mm-thick	Si, Zn, and Ni powders	Steel on top, special clamping device, orthogonal design of experiment involving laser power, welding speed, defocusing and gas flow	103 N/mm (approx.) max. tensile resistance	Fe_2Al_5, $FeAl_3$	[65]
	CW fiber laser, 4 kW max. power	6061 1 mm-thick	DP590 (galvanized) 1 mm-thick	None	Steel on top, application of a magnetic field to improve microstructure	1.22 kN max. shear load	Fe_2Al_5, $FeAl_3$, $Fe_{46.22}Al_{192.4}$	[81]
	CW fiber laser, 10 kW max. power	7075 1 mm-thick	DP590 (galvanized) 1.2 mm-thick	None	Aluminum on top, dual beam: 80% power density main beam (on aluminum), 20% derived beam (on steel)	123.7 MPa max. tensile strength	Fe_2Al_5, $FeAl_3$	[69]
	PW Nd:YAG laser, 12 kW max. peak power	1050 1 mm-thick	DP1000 1 mm-thick	None	Steel on top, two parallel welding beads with pulsed laser varying laser power, pulse duration, overlapping, defocusing and welding speed	123 MPa max. tensile strength	Not reported	[74]
	CW fiber laser, 4 kW max. power	5052 2 mm-thick	DP780 2 mm-thick	None	Steel on top, variation of processing parameters to optimize mechanical performance	1964 N max. shear load	$FeAl_2$, Fe_2Al_5, $FeAl_3$	[75]

Table 2. *Cont.*

Joint Type	Laser System	Aluminum Alloy	Steel	Filler Metal	Joining Approach	Mechanical Properties	Reported IMCs	Ref.
	CW fiber laser, 5 kW max. power	5052 2 mm-thick	Q235 (galvanized) 1.8 mm-thick	ZnAl22 flux-cored wire	Aluminum on top, laser spot both on steel and aluminum (i.e., fillet weld in a lap joint)	1.22 kN max. shear load	FeAl, FeZn10, $Fe_2Al_{5-x}Zn_x$	[70]
	CW fiber laser, 6 kW max. power	6061 1.5 mm-thick	CR340 1.2 mm-thick	Al-12%Si flux-cored wire	Aluminum on top, laser spot both on steel and aluminum (i.e., fillet weld in a lap joint), different welding gases (CO_2, Ar, CO_2+Ar)	163 MPa max. tensile-shear strength	$Fe_2(Al,Si)_5$, $Fe(Al,Si)_3$, $Fe_{1.8}Al_{7.2}Si$	[55]
	CW fiber laser, 6 kW max. power	5052 1 mm-thick	SPCC (galvanized) 1 mm-thick	Al-2%Si flux-cored wire	Aluminum on top, use of a jig to tilt the joint and improve wettability and Ti interlayer to reduce porosity	185 MPa max. tensile-shear strength	$FeAl_3$, $FeZn_3$, $FeZn_8$	[78]
	CW diode laser, 6 kW max. power	6061 3 mm-thick	DP600 2.5 mm-thick	None	Steel on top, controlling interaction time and power density to obtain desired weld penetration and microstructure	231 MPa max. tensile-shear strength	Fe_2Al_5, $FeAl_3$	[72]
	CW diode laser, 2.5 kW max. power	6061 1.5 mm-thick	AISI 304 1.5 mm-thick	$CoZnCuMn_{0.8}Si_{0.2}$, FeCoCrNiMn high-entropy powders, and commercial Al-12%Si powder	Application of high-entropy powders to inhibit IMC formation and growth (coaxial powder feeding)	Not reported	FeAl, Fe_4Al_{13}	[79]
	CW fiber laser, 6 kW max. power	6061 2 mm-thick	304 stainless steel 2 mm-thick	None	Steel on top, oscillating laser beam	185 N/m max. tensile-shear resistance	Fe_2Al_5, Fe_4Al_{13}	[71]

Table 2. *Cont.*

Joint Type	Laser System	Aluminum Alloy	Steel	Filler Metal	Joining Approach	Mechanical Properties	Reported IMCs	Ref.
	CW fiber laser, 5 KW max. power	6061 2 mm-thick	Q235 (galvanized) 2 mm-thick	ER4043 solid wire	Aluminum on top, tilted wire feeding, Cu backing plate	70.4 MPa max. tensile strength	$Fe_2Al_5Zn_{0.4}$, $Fe_3Al_{0.5}Si_{0.5}$, $Fe_3Al_{0.7}Si_{0.3}$	[58]
	CW fiber laser, 6 kW max. power	6061 1.5 mm-thick	22MnB5 1.9 mm-thick	ZnAl15 solid wire	Aluminum on top, different defocusing distances to widen processing parameters windows	2793 N max. shear load	$Fe_2(Al,Zn)_5$, $FeZn_{10}$	[60]
	CW fiber laser, 4 kW max. power	6061 1 mm-thick	DP590 (galvanized) 1 mm-thick	ZnAl15 solid wire	Aluminum on top, application of external alternating magnetic field	2.26 kN max. shear load	$Al_5Fe_2Zn_{0.4}$, $FeZn_{10}$, ZnAl	[82]
Butt	CW fiber laser, 10 kW max. power	6061 2 mm-thick	Q235 (galvanized) 2 mm-thick	ER4043 solid wire	60° bevel angle at aluminum, 30° and 45° bevel angle at steel	150 MPa max. tensile strength	Fe_2Al_5, $FeAl_3$	[84]
	CW fiber laser, 6 kW max. power	6061 1.5 mm-thick	DP590 1.2 mm-thick	ER1100, ER4043, ER4047 solid wires	45° bevel angle at steel side, 1.0 mm root opening (gap)	204 MPa max. tensile strength	Fe_2Al_5, $FeAl_3$, $Fe_2(Al,Si)_5$, $Fe(Al,Si)_3$, Fe_2Al_8Si	[87]
	CW fiber laser, 10 kW max. power	6061 2 mm-thick	DP590 2 mm-thick	Al-12%Si flux-cored wire	Different combinations of beveling aluminum and steel, respectively:1) half-V and square; 2) half-Y and half-Y; 3) half-Y and half-V	145.8 MPa max. tensile strength	$Fe(Al,Si)_3$, $Fe_{1.8}Al_{7.2}Si$	[85]
	CW fiber laser, 6 kW max. power	6061 2 mm-thick	DP590 2 mm-thick	Al-12%Si flux-cored wire	45° bevel angle at both sides, 1.0 mm root opening (gap)	140 MPa max. tensile strength	$Fe(Al,Si)_3$, $Fe_2(Al,Si)_5$, $Fe_{1.8}Al_{7.2}Si$	[86]
	CW fiber laser, 6 kW max. power	6061 1.5 mm-thick	DP590 1.2 mm-thick	ZnAl2, ZnAl15 and ZnAl22 flux-cored wires	45° bevel angle at aluminum side, 1.0 mm root opening (gap)	274 MPa max. tensile strength	$FeZn_{10}$, $Fe_2Al_5Zn_{0.4}$	[88]

Table 2. *Cont.*

Joint Type	Laser System	Aluminum Alloy	Steel	Filler Metal	Joining Approach	Mechanical Properties	Reported IMCs	Ref.
	CW fiber laser, 4 kW max. power (in combination with Cold Metal Transfer arc welding)	5052 2 mm-thick	Q235 2 mm-thick	ER5356 solid wire	Hybrid laser-CMT (laser-leading configuration)	83.4 MPa max. tensile strength	Fe_2Al_5, Fe_4Al_{13}	[92]
	CW fiber laser, 6 kW max. power	6061 2 mm-thick	DP590 2 mm-thick	AlSi10Mg powder	45° bevel angle at both sides, two layers of powder deposition inside an Ar chamber	194 MPa max. tensile strength	$Fe(Al,Si)_3$, $Fe_2(Al,Si)_5$, $Fe_{1.8}Al_{7.2}Si$	[16]
	CW fiber laser, 5 kW max. power	6061 2 mm-thick	DP590 2 mm-thick	ER4047 solid wire	45° bevel angle at both sides, 0.6 mm root opening (gap), dual laser beam (cross and in-line)	196 MPa max. tensile strength	$Fe(Al,Si)_3$, $Fe_2(Al,Si)_5$, $Fe_{1.8}Al_{7.2}Si$	[90]
	CW fiber laser, 6 kW max. power (in combination with Cold Metal Transfer arc welding)	6061 2.1 mm-thick	AISI304 1.8 mm-thick	ER4043 solid wire	Hybrid laser-CMT (laser-leading configuration), circular beam oscillation (offset oscillation)	160 MPa max. tensile strength	Fe_2Al_5, Fe_4Al_{13}	[93]
	CW fiber laser, 1.20 kW max. mean power	7075 1 mm-thick	D6AC 1 mm-thick	None	Direct laser beam welding, laser spot in the middle of the joint melting both materials	94 MPa max. tensile strength	$FeAl_3$, Fe_3Al, Fe_2Al_5	[94]
	CW fiber laser, 3 kW max. power	6061 1.6 mm-thick	S235 1.5 mm-thick	ER4043 solid wire and Al-12%Si preplaced powder	Welding wire (tilted 45° from joint axis towards steel) in combination with preplaced powder	169 MPa max. tensile strength	Fe_2Al_5, Fe_4Al_{13}, $Fe_4Al_{17.5}Si_{1.5}$	[89]

As one can see in Table 2, most of the researchers have used thin sheets (up to 2 or 3 mm, with rare exceptions), as one should expect due to the interest in lightweight structures. The most common aluminum alloys used in dissimilar aluminum–steel joints belong to 5xxx and 6xxx series, which are the most commonly used aluminum alloys for automotive and aircraft applications. On the other hand, steels used in these studies are as diverse as mild steels, stainless steels and high strength steels. Additionally, some of them are galvanized. Although different filler metals have been applied, the most common choice is Al-Si wire, due to the known capacity of these alloys to reduce Fe-Al IMC layer thickness. Interestingly, regardless of the combination of aluminum alloy, steel and filler metal used, the dissimilar joints usually show very similar intermetallics and also comparable mechanical properties.

4. Microstructural Features of IMCs within Dissimilar Aluminum–Steel Joints

As already discussed, the intermetallic compounds (IMC) layer formed at the interface between dissimilar materials is the weakest region of dissimilar joints. Thus, most of the research efforts in laser joining of aluminum to steel have been focused on controlling IMC formation and growth. On the other hand, the mechanisms of formation and growth of IMCs are still not clear, although several authors have obtained dissimilar aluminum–steel joints with very thin IMC layers and relatively good mechanical properties. In this section, the formation and growth of intermetallic compounds within dissimilar aluminum–steel joints are reviewed. It is worth mentioning that several published research works aiming at understanding these mechanisms were performed by carrying out hot dipping experiments (solid steel sheets in molten aluminum baths) or aluminum–steel diffusion couples, as these experimental configurations provide more means to study the involved phenomena (easy control of reactions time and temperature, flexibility of bath compositions, possibility of changing parameters without compromising the stability of process, etc.) than welding experiments themselves. Although these experimental configurations are not identical to the actual welding process due to the very short times involved and very high-temperature gradients characteristic of welding, they provide useful information on the formation and growth of IMCs.

Rong et al. [95] studied the growth kinetics of Fe-Al IMCs by submitting pure Al-Q235 steel couples to controlled thermal cycles using a thermophysical simulation methodology. The aim of the authors was to simulate the actual welding conditions (peak temperature from 700 to 900 $^\circ$C and holding time at peak temperature up to 9 s). They observed the formation of predominant Fe_2Al_5 adjacent to the steel, and when peak temperature increased the layer was thicker and its morphology changed from tongue-like to wavy. Figure 14 illustrates how IMC layer thickness and morphology change with dipping temperature.

A thinner Fe_4Al_{13} layer was found adjacent to the aluminum, and when peak temperature exceeded 800 $^\circ$C, small free-morphology islands of Fe_4Al_{13} were detected inside the Al matrix. Figure 15 illustrates the appearance of the resulting IMC layer, showing commonly found Fe-Al IMCs such as Fe_2Al_5 (η) and Fe_4Al_{13} (θ), and a line scan chemical analysis carried out by Energy Dispersive X-Ray Spectroscopy (EDS).
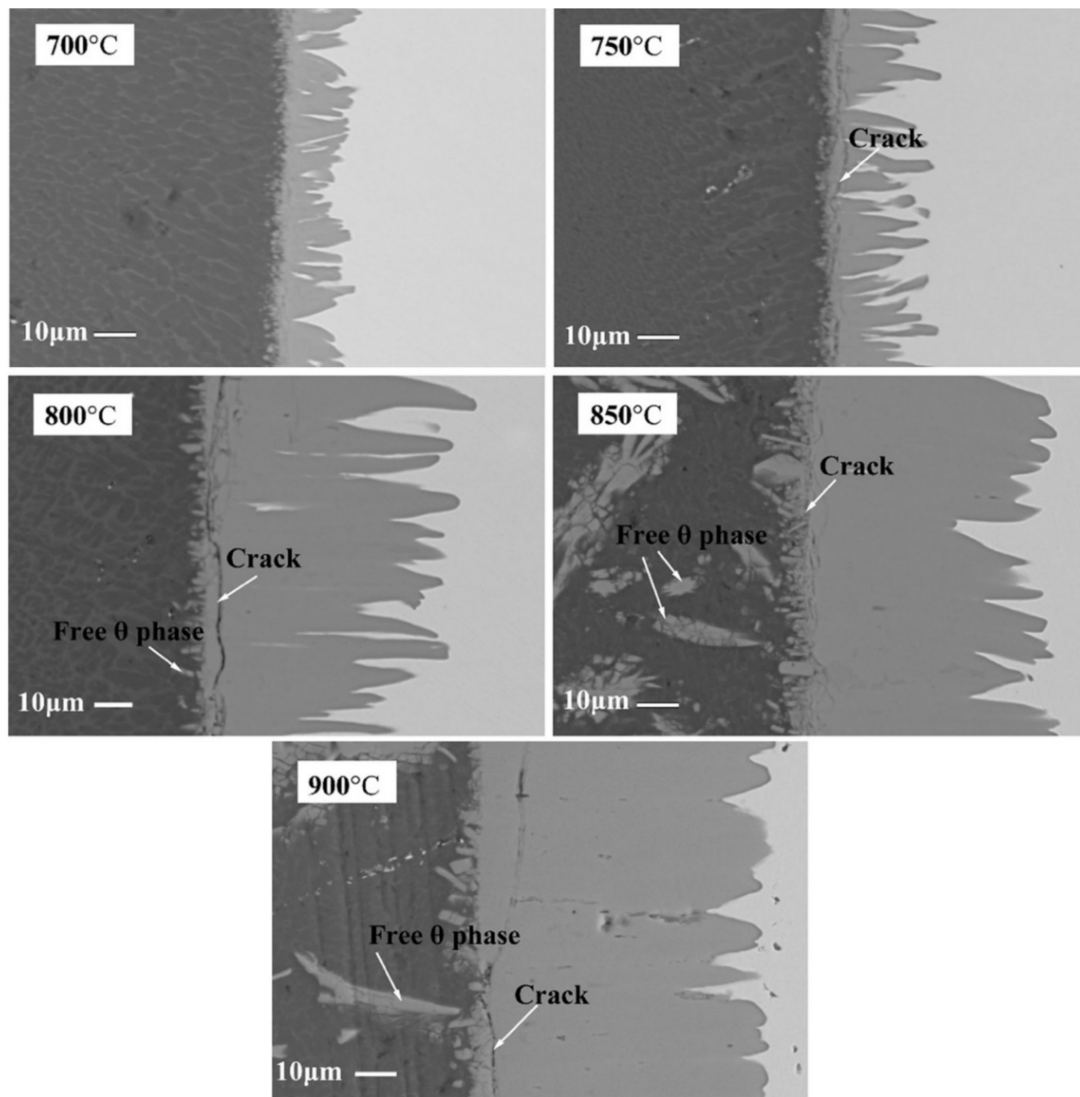
Figure 14. The dependence of IMC thickness on dipping peak temperature. Holding time for all samples was 5 s. Reproduced from Rong et al. (Reprinted with permission from ref. [95]. Copyright 2017 Elsevier).
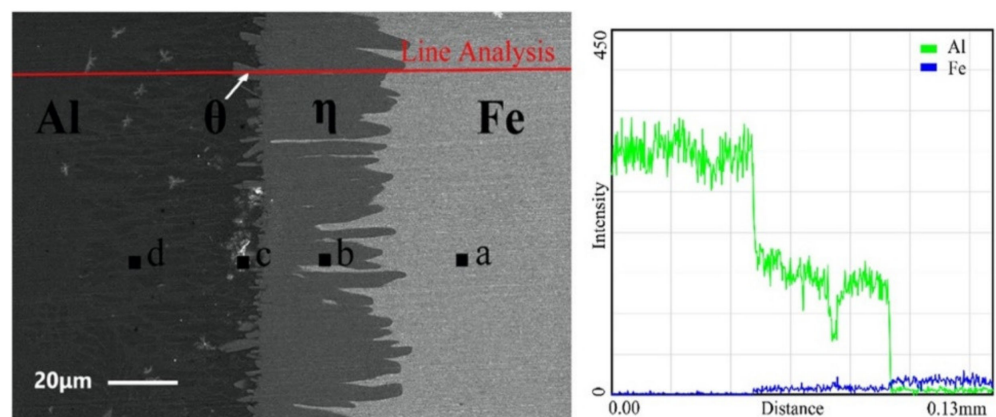

Figure 15. Intermetallic compounds commonly seen in dissimilar aluminum–steel joints, and the line scan chemical composition analysis for Al and Fe elements. (Reprinted with permission from ref. [95]. Copyright 2017 Elsevier).

The authors proposed that Fe_2Al_5 growth is controlled by a mixed mechanism, both by interfacial reaction and diffusion. The growth in the *c*-axis direction would be predominantly governed by interfacial reactions, and the growth in other directions would be mainly controlled by diffusion. Additionally, the Fe_2Al_5 thickness would depend more strongly on interfacial reactions when reaction time is short, and more strongly on diffusion at longer reaction times. In turn, Fe_4Al_{13} would nucleate heterogeneously at the aluminum–steel interface during cooling, explaining the needle-like morphology at the interface. On the other hand, Fe atoms that diffused into Al matrix apart from the interface give room to homogeneous nucleation of Fe_4Al_{13}, originating the free-morphology islands seen in Figure 14.

He et al. [96] calculated the Gibbs free energy of formation for Fe-Al IMCs from approximately 650 to 1200 °C, and found that Fe_4Al_{13}, $FeAl_3$ and Fe_2Al_5 show the lowest energy values within this temperature range, which explains the common formation of these IMCs. By carrying out hot dipping experiments of Q235 mild steel in AA1050 aluminum bath, they observed the formation of Fe_2Al_5 and Fe_4Al_{13}, and assessed separately the formation and growth of each IMC. They stated that Fe_2Al_5 seems to obey a parabolic rate law, showing a considerable increase in thickness both when dipping temperature and time increased. In turn, Fe_4Al_{13} thickness decreased both when dipping temperature increased from 700 to 900 °C, and when dipping time increased from 2 to 10 s, although the thickness variations of Fe_4Al_{13} were slighter than Fe_2Al_5 ones. The authors related the thickness decrease to the dissolution of Fe_4Al_{13}, suggesting that Fe_4Al_{13} growth kinetics is ruled by interfacial reactions.

Effect of Aluminum Alloy Composition

Some authors have studied the influence of bath composition for hot dipping experiments of steel sheets into aluminum alloy baths. Although the conditions are not exactly the same as those of a welding process, they can assist the understanding of the influence of filler metal composition and welding dilution. Therefore, relevant works on the influence of bath composition in hot dipping experiments are reviewed below.

Takata et al. [97] studied hot dipping of pure Fe sheets in pure Al and in Al-8.2%Mg-4.8%Si baths. Although the same IMCs (Fe_2Al_5 and $FeAl_3$) were found in all conditions, the samples dipped into the Al-Mg-Si bath showed much thinner IMC layers. The authors stated that the growth kinetics of Fe_2Al_5 was approximately ten times faster in pure Al baths than in the Al-Mg-Si bath, which they related to the continuous $FeAl_3$ layer acting as a diffusion barrier. In pure Al baths, the $FeAl_3$ layer was discontinuous, providing a solid–liquid contact interface, which results in much faster IMC growth. $FeAl_3$ layer was also thicker in pure Al baths than in Al-Mg-Si ones, but the difference in thickness was not so relevant as in the case of Fe_2Al_5. Lastly, the authors found up to 3 at. % Si in solid solution within both IMCs in the IMC layer while no Mg was detected, indicating that Si atoms are more likely to enter the IMC sublattices as a substitutional atom. The significant differences in the dimensions and morphology between the IMC layers in pure Al and in Al-Mg-Si baths are shown in Figure 16a,b, while phase maps obtained by Electron Backscattered Diffraction (EBSD) are shown in Figure 16c,d.
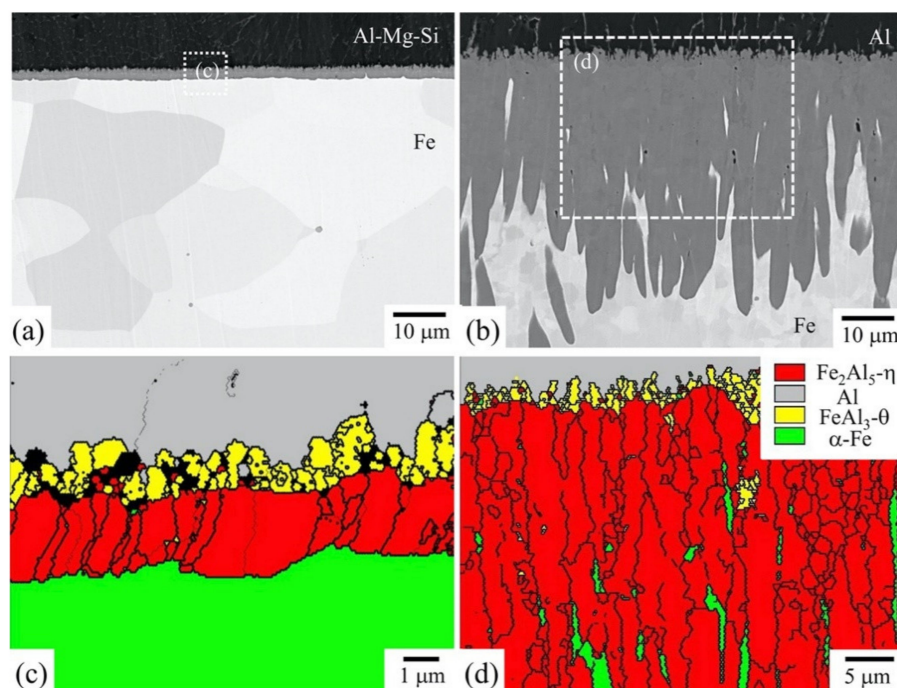
Figure 16. Intermetallic compounds (IMC) layers reported by Takata et al. for Fe sheets dipped at 750 °C for 60 s in (**a**,**c**) Al-Mg-Si bath; (**b**,**d**) pure Al bath. (Reprinted with permission from ref. [97]. Copyright 2014 Elsevier).

Cheng and Wang [98] studied hot dipping of low-carbon steel in pure Al and in Al-Si baths with different concentrations of Si (0.5, 2.5, 5 and 10%Si) at 700 °C for 180 s, followed by cooling in static air. They stated that the IMC layer thickness decreased with an increase in Si content. Additionally, they reported the formation of ternary Fe-Al-Si IMCs (besides binary Fe-Al ones) and the transformation of the IMC morphology from tongue-like into a flat morphology/y when Si content was higher than 2.5%. The authors also reported the formation of metastable $Al_7(Fe,M)_2Si$ (M = Mn, Cr or Cu) when Si content was up to 5%, and the occurrence of Al_7Fe_2Si when Si content was higher than 5%. Although both IMCs seem to take place by the same mechanism, the metastable ternary IMC is more likely to form in fast solidification conditions. The authors explained that, when Si content approaches 10%, the melting temperature of the bath decreases (the eutectic composition of Al-Si alloys is 12%Si), and so do the cooling rates, as the cooling departs from the same temperature in all experiments independently of the Si content. It is interesting to notice the synergic effect that takes place when modifications in the chemical composition of the bath influence the cooling rates, although the global experiment thermal cycle is exactly the same.

Although the effects of Si on IMC thickness have been reported by several authors, the mechanism by which Si suppresses the IMC layer growth is still not clear. Several authors claim that Si occupies vacancy sites in the *c*-axis of Fe_2Al_5 phase and impedes the IMC layer growth by blocking diffusion [15,99–101]. However, Springer et al. [102] earlier showed experimental evidence that contradicts this hypothesis, as they found Fe_2Al_5 layer in solid steel/semi-solid Al-5%Si diffusion couples at 600 °C were thicker than Fe_2Al_5 layer formed in steel/pure aluminum couples at the same temperature. Later, Lemmens et al. [103] observed Fe_2Al_5 layer in steel samples hot-dipped into Al-10%Si at 670 °C were thicker than at 725 °C, and also questioned the diffusion-blocking mechanism. It is clear that further research is needed in order to clarify the IMC growth suppression by Si and other alloying elements.

5. Discussion, Conclusions and Future Prospects

Laser welding is an advanced joining process that provides high flexibility, accurate control of heat input, and fast cooling rates. Due to its characteristics, laser welding has become an interesting choice when it comes to joining dissimilar materials, yet it still has to evolve in order to achieve wide acceptance by industry.

We believe that the poor comprehension of complex phenomena involved in laser joining of aluminum to steel, and also the limited mechanical performance of resulting joints are important reasons why the application of this technique in the industry is still modest. There are several scientific issues that still remain unsolved and need to be further investigated. In order to obtain high-performance aluminum–steel joints, it is highly desirable to control as much as possible the formation of imperfections, and to maximize the wettability of aluminum on steel. However, there are no general rules that could lead us to the optimal processing conditions. Although there are many parameters involved in a particular laser joining configuration, the most commonly studied processing parameters are laser power, beam diameter, welding speed, and wire feed speed (when wire is present). Although they can be adjusted individually, there are important interactions between them, in such a way that usually the parameters have to be adjusted simultaneously: for example, in order to increase wire feeding, laser power has to be also increased to guarantee enough wire melting. Such interactions bring difficulty to the joining process operation, and, in fact, can increase together with the complexity of the joining approach itself. Additionally, some competitive effects that have been presented throughout this review are inherent to the joining process: for instance, higher laser power leads to improvements in wettability and wire melting, but can thicken the IMC layer, undesirably melt the steel, cause welding imperfections such as sagging and burn-through, and increase zinc evaporation. Therefore, the right balance has to be achieved, and this is normally a challenging and time-consuming task.

One possible way to deal with the high quantity of parameters is to consider combinations of them: power density (laser power divided by the beam area at the material's surface) [104,105], interaction time (beam diameter divided by welding speed) [104,105], and specific point energy (laser power times interaction time) [106] have been introduced by different authors and can help us with transferability and repeatability [107]. However, combined parameters unfortunately are not commonly considered in the context of aluminum–steel laser joining.

The IMC layer is usually the weakest part of the dissimilar joint, and failure commonly takes place within it. Therefore, most of the researchers' efforts have been put on controlling the IMC layer in order to produce high-performance dissimilar joints, yet so far only limited-strength joints have been obtained due to the brittle behavior of IMCs.

As presented throughout this review, the current state of the art of laser joining approaches could be classified into two groups: approaches based on thorough control of thermal cycles, and approaches based on chemical modifications. The most important issues in the former group are related to controlling diffusion time and peak temperature, as these two parameters influence IMC formation and growth in a determinant way. In the latter group, in turn, chemical modifications are imposed to the weld pool aiming at controlling the resulting IMC layer thickness and morphology. These chemical modifications are usually achieved by using different combinations of filler metals (wire, powder, or both) and fluxes. Obviously, a particular approach may have characteristics of both groups, as the welding conditions are usually selected taking the IMC into account, and a filler metal is commonly used. Additionally, some particular approaches have characteristics that do not fit precisely into this classification. Anyway, we believe that the first group has been much more explored than the second one. Although the mechanisms of IMC layer formation and growth are still unclear, there is, to a certain extent, considerable comprehension of the influence of thermal cycles on the resulting IMC layer characteristics. On the other hand, there is still room for advancements by investigating new combinations of existing filler metals and fluxes, not to mention the development of new chemical compositions, aiming

at obtaining favorable IMC layer modifications that would lead to higher mechanical performance. Unfortunately, these approaches usually involve arrangements such as modified beam shapes and waves, oscillating beams, advanced clamping devices, non-conventional filler metals, powder deposition systems, and beveling the sheets. Although the complexity of such approaches is intentionally introduced aiming at improving microstructure and mechanical properties of resulting joints, welding costs, time and operation difficulty are increased along with the complexity of these joining approaches, limiting the acceptance of the technology by the industry.

Although considerable achievements have been obtained, comprehension of phenomena involved in IMC formation and growth in the context of dissimilar laser joining is still limited. The deepest studies available regarding this issue have been carried out in hot dipping or diffusion-couple experiments. Yet useful, these studies do not reproduce the conditions under which a laser welding process takes place. While many authors focused on the mechanical properties of the joints, the physical phenomena behind IMC formation and growth are still unclear.

An important step towards understanding IMC formation and growth is accurate phase identification. Most of the research works on aluminum–steel laser joining have identified IMC based only on EDS and sometimes X-ray diffraction (XRD) analyses. Particularly, the EDS technique shows an important flaw: unwanted material underneath the surface is also analyzed due to the pear-shaped interaction volume inherent to the technique [108]. Thus, although usually the chemical analyses obtained by EDS are unquestionably considered, they should be carried out carefully. More refined techniques such as EBSD, transmission electron microscopy (TEM), selected area electron diffraction (SAED), integral low-energy electron Mössbauer spectroscopy (ILEEMS), and electron energy loss spectroscopy (EELS) are not commonly used, although they potentially lead to much more accurate results. Indeed, different characterization techniques should be combined, complementing each other to increase the reliability of results. Moreover, the employment of real-time monitoring technology potentially connected to adaptative control systems [109], which have been successfully employed in laser welding systems, could bring more advancements to dissimilar joining applications. Lastly, thermo-mechanical and multi-physical simulations [110] are also expected to be further explored, although some models have already been developed by these means [71,111–113].

Considering the exposure, we expect on the one hand the development of trustworthy, relatively simple and affordable approaches to obtain high-performance dissimilar joints. We hope novel approaches will provide an appropriate balance between wettability, absence of imperfections and suitable microstructure (particularly IMC thickness), still maintaining costs and complexity to limited levels. On the other hand, we also expect further scientific improvements in understanding IMC formation and growth, and the influence of welding thermal cycles and filler metals on it. We wish that future research on laser welding will focus not only on obtaining high-performance joints, but also on further clarifying the phenomena involved in IMC formation and growth in specific welding conditions. To this end, we expect that researchers' attention will not only be put on mechanical properties, but also on improving our comprehension of the issues presented throughout this review.

In conclusion, further research is expected to be carried out in the near future in order to promote the consolidation of laser welding as a reliable joining process applied to dissimilar materials. It is expected that the formation and growth of intermetallic compounds at the interface of aluminum–steel welds will be further clarified, providing mains to manage the microstructural features of the joints. Additionally, more effort is expected so as to promote transferability and repeatability of the technology. Finally, it is expected that this knowledge will lead to the development of new laser joining approaches in order to provide high-performance dissimilar joints at a reasonable cost, promoting future broad acceptance of this technology by the industry.

References

1. Rissman, J.; Bataille, C.; Masanet, E.; Aden, N.; Morrow, W.R.; Zhou, N.; Elliott, N.; Dell, R.; Heeren, N.; Huckestein, B.; et al. Technologies and policies to decarbonize global industry: Review and assessment of mitigation drivers through 2070. *Appl. Energy* **2020**, *266*, 114848. [CrossRef]

2. Allwood, J.M.; Ashby, M.F.; Gutowski, T.G.; Worrell, E. Material efficiency: Providing material services with less material production. *Philos. Trans. R. Soc. A Math. Phys. Eng. Sci.* **2013**, *371*, 20120496. [CrossRef]

3. Bayock, F.N.; Kah, P.; Salminen, A.; Belinga, M.; Yang, X. Feasibility study of welding dissimilar Advanced and Ultra High Strength Steels. *Rev. Adv. Mater. Sci.* **2020**, *59*, 54–66. [CrossRef]

4. Carruth, M.A.; Allwood, J.M.; Moynihan, M.C. The technical potential for reducing metal requirements through lightweight product design. *Resour. Conserv. Recycl.* **2011**, *57*, 48–60. [CrossRef]

5. Wargnier, H.; Kromm, F.X.; Danis, M.; Brechet, Y. Proposal for a multi-material design procedure. *Mater. Des.* **2014**, *56*, 44–49. [CrossRef]

6. Sakundarini, N.; Taha, Z.; Abdul-Rashid, S.H.; Ghazila, R.A.R. Optimal multi-material selection for lightweight design of automotive body assembly incorporating recyclability. *Mater. Des.* **2013**, *50*, 846–857. [CrossRef]

7. Raabe, D.; Tasan, C.C.; Olivetti, E.A. Strategies for improving the sustainability of structural metals. *Nature* **2019**, *575*, 64–74. [CrossRef] [PubMed]

8. Bajaj, P.; Hariharan, A.; Kini, A.; Kürnsteiner, P.; Raabe, D.; Jägle, E.A. Steels in additive manufacturing: A review of their microstructure and properties. *Mater. Sci. Eng. A* **2020**, *772*, 138633. [CrossRef]

9. Tomków, J.; Rogalski, G.; Fydrych, D.; Łabanowski, J. Improvement of S355G10 + N steel weldability in water environment by Temper Bead Welding. *J. Mater. Process. Technol.* **2018**, *262*, 372–381. [CrossRef]

10. Ashkenazi, D. How aluminum changed the world: A metallurgical revolution through technological and cultural perspectives. *Technol. Forecast. Soc. Change* **2019**, *143*, 101–113. [CrossRef]

11. Shah, L.H.; Ishak, M. Review of Research Progress on Aluminum–Steel Dissimilar Welding. *Mater. Manuf. Process.* **2014**, *6914*, 928–933. [CrossRef]

12. Hussein, S.A.; Tahir, A.S.M.; Hadzley, A.B. Characteristics of aluminum-to-steel joint made by friction stir welding: A review. *Mater. Today Commun.* **2015**, *5*, 32–49. [CrossRef]

13. Bouayad, A.; Gerometta, C.; Belkebir, A.; Ambari, A. Kinetic interactions between solid iron and molten aluminium. *Mater. Sci. Eng. A* **2003**, *363*, 53–61. [CrossRef]

14. Song, J.L.; Lin, S.B.; Yang, C.L.; Fan, C.L. Effects of Si additions on intermetallic compound layer of aluminum–steel TIG welding–brazing joint. *J. Alloys Compd.* **2009**, *488*, 217–222. [CrossRef]

15. Singh, J.; Arora, K.S.; Shukla, D.K. Dissimilar MIG-CMT weld-brazing of aluminium to steel: A review. *J. Alloys Compd.* **2019**, *783*, 753–764. [CrossRef]

16. Xia, H.; Zhang, L.; Tan, C.; Wu, L.; Chen, B.; Li, L. Effect of heat input on a laser powder deposited Al/steel butt joint. *Opt. Laser Technol.* **2019**, *111*, 459–469. [CrossRef]

17. Unt, A.; Poutiainen, I.; Grünenwald, S.; Sokolov, M.; Salminen, A. High Power Fiber Laser Welding of Single Sided T-Joint on Shipbuilding Steel with Different Processing Setups. *Appl. Sci.* **2017**, *7*, 1276. [CrossRef]

18. Landowski, M.; Świerczyńska, A.; Rogalski, G.; Fydrych, D. Autogenous Fiber Laser Welding of 316L Austenitic and 2304 Lean Duplex Stainless Steels. *Materials* **2020**, *13*, 2930. [CrossRef]

19. Liedl, G.; Vázquez, R.G.; Murzin, S.P. Joining of Aluminium Alloy and Steel by Laser Assisted Reactive Wetting. *Lasers Manuf. Mater. Process.* **2018**, *5*, 1–15. [CrossRef]

20. Meco, S.; Cozzolino, L.; Ganguly, S.; Williams, S.; McPherson, N. Laser welding of steel to aluminium: Thermal modelling and joint strength analysis. *J. Mater. Process. Technol.* **2017**, *247*, 121–133. [CrossRef]

21. Liu, X.; Dong, Q.; Wang, P.; Chen, H. Review of Electron Beam Welding Technology in Space Environment. *Optik* **2021**, *225*, 165720. [CrossRef]

22. Dinda, S.K.; Kar, J.; Jana, S.; Gopal Roy, G.; Srirangam, P. Effect of beam oscillation on porosity and intermetallics of electron beam welded DP600-steel to Al 5754-alloy. *J. Mater. Process. Technol.* **2019**, *265*, 191–200. [CrossRef]

23. Bogue, R. Fifty years of the laser: Its role in material processing. *Assem. Autom.* **2010**, *30*, 317–322. [CrossRef]

24. Li, Y.; Chen, C.; Yi, R.; Ouyang, Y. Review: Special brazing and soldering. *J. Manuf. Process.* **2020**, *60*, 608–635. [CrossRef]

25. Klocke, F.; Castell-Codesal, A.; Donst, D. Process Characteristics of Laser Brazing Aluminium Alloys. *Adv. Mater. Res.* **2005**, *6–8*, 135–142. [CrossRef]

26. Kashaev, N.; Ventzke, V.; Çam, G. Prospects of laser beam welding and friction stir welding processes for aluminum airframe structural applications. *J. Manuf. Process.* **2018**, *36*, 571–600. [CrossRef]

27. Wan, L.; Huang, Y. Friction stir welding of dissimilar aluminum alloys and steels: A review. *Int. J. Adv. Manuf. Technol.* **2018**, *99*, 1781–1811. [CrossRef]

28. Heidarzadeh, A.; Mironov, S.; Kaibyshev, R.; Çam, G.; Simar, A.; Gerlich, A.; Khodabakhshi, F.; Mostafaei, A.; Field, D.P.; Robson, J.D.; et al. Friction stir welding/processing of metals and alloys: A comprehensive review on microstructural evolution. *Prog. Mater. Sci.* **2020**, *117*, 100752. [CrossRef]

29. Cao, X.; Wallace, W.; Immarigeon, J.-P.; Poon, C. Research and Progress in Laser Welding of Wrought Aluminum Alloys: II. Metallurgical Microstructures, Defects, and Mechanical Properties. *Mater. Manuf. Process.* **2003**, *18*, 23–49. [CrossRef]

30. Li, W.; Vairis, A.; Preuss, M.; Ma, T. Linear and rotary friction welding review. *Int. Mater. Rev.* **2016**, *61*, 71–100. [CrossRef]

31. Kumar Rajak, D.; Pagar, D.D.; Menezes, P.L.; Eyvazian, A. Friction-based welding processes: Friction welding and friction stir welding. *J. Adhes. Sci. Technol.* **2020**, *34*, 2613–2637. [CrossRef]

32. Kovacs-Coskun, T.; Volgyi, B.; Sikari-Nagl, I. Investigation of aluminum-steel joint formed by explosion welding. *J. Phys. Conf. Ser.* **2015**, *602*, 012026. [CrossRef]

33. Carvalho, G.H.S.F.L.; Galvão, I.; Mendes, R.; Leal, R.M.; Loureiro, A. Aluminum-to-Steel Cladding by Explosive Welding. *Metals* **2020**, *10*, 1062. [CrossRef]

34. Findik, F. Recent developments in explosive welding. *Mater. Des.* **2011**, *32*, 1081–1093. [CrossRef]

35. Moskvitin, G.V.; Polyakov, A.N.; Birger, E.M. Application of laser welding methods in industrial production. *Weld. Int.* **2013**, *27*, 572–580. [CrossRef]

36. Wang, P.; Chen, X.; Pan, Q.; Madigan, B.; Long, J. Laser welding dissimilar materials of aluminum to steel: An overview. *Int. J. Adv. Manuf. Technol.* **2016**, 1–10. [CrossRef]

37. Wang, J.; Fu, X.; Zhang, L.; Zhang, Z.; Liu, J.; Chen, S. A short review on laser welding/brazing of aluminum alloy to steel. *Int. J. Adv. Manuf. Technol.* **2021**, *112*, 2399–2411. [CrossRef]

38. Bunaziv, I.; Akselsen, O.M.; Salminen, A.; Unt, A. Fiber laser-MIG hybrid welding of 5 mm 5083 aluminum alloy. *J. Mater. Process. Technol.* **2016**, *233*, 107–114. [CrossRef]

39. Sierra, G.; Peyre, P.; Deschaux-Beaume, F.; Stuart, D.; Fras, G. Steel to aluminium key-hole laser welding. *Mater. Sci. Eng. A* **2007**, *447*, 197–208. [CrossRef]

40. Çam, G.; İpekoğlu, G. Recent developments in joining of aluminum alloys. *Int. J. Adv. Manuf. Technol.* **2016**, *91*, 1851–1866. [CrossRef]

41. Cao, X.; Wallace, W.; Poon, C.; Immarigeon, J.-P. Research and Progress in Laser Welding of Wrought Aluminum Alloys: I. Laser Welding Processes. *Mater. Manuf. Process.* **2003**, *18*, 1–22. [CrossRef]

42. Ai, Y.; Shao, X.; Jiang, P.; Li, P.; Liu, Y.; Liu, W. Welded joints integrity analysis and optimization for fiber laser welding of dissimilar materials. *Opt. Lasers Eng.* **2016**, *86*, 62–74. [CrossRef]

43. Guan, Y.; Sun, S.; Zhao, G.; Luan, Y. Influence of material properties on the laser-forming process of sheet metals. *J. Mater. Process. Technol.* **2005**, *167*, 124–131. [CrossRef]

44. Hong, K.-M.; Shin, Y.C. Prospects of laser welding technology in the automotive industry: A review. *J. Mater. Process. Technol.* **2017**, *245*, 46–69. [CrossRef]

45. Gao, M.; Chen, C.; Mei, S.; Wang, L.; Zeng, X. Parameter optimization and mechanism of laser-arc hybrid welding of dissimilar Al alloy and stainless steel. *Int. J. Adv. Manuf. Technol.* **2014**, *74*, 199–208. [CrossRef]

46. ASM International. Welding, brazing and soldering. In *ASM Handbook*; Olson, D.L., Siewert, T.A., Liu, S., Edwards, G.R., Eds.; ASM International: Novelty, OH, USA, 1993; ISBN 978-1-62708-173-3.

47. ASM International. *Metals Handbook Desk Edition*; Davis, J.R., Ed.; ASM International: Novelty, OH, USA, 1998; ISBN 978-1-62708-199-3.

48. Agudo, L.; Eyidi, D.; Schmaranzer, C.H.; Arenholz, E.; Jank, N.; Bruckner, J.; Pyzalla, A.R. Intermetallic Fe_xAl_y-phases in a steel/Al-alloy fusion weld. *J. Mater. Sci.* **2007**, *42*, 4205–4214. [CrossRef]

49. Zhang, Y.; Guo, G.; Li, F.; Wang, G.; Wei, H. The interface control of butt joints in laser braze welding of aluminium-steel with coaxial powder feeding. *J. Mater. Process. Technol.* **2017**, *246*, 313–320. [CrossRef]

50. Novák, P.; Michalcová, A.; Marek, I.; Mudrová, M.; Saksl, K.; Bednarčík, J.; Zikmund, P.; Vojtěch, D. On the formation of intermetallics in Fe–Al system—An in situ XRD study. *Intermetallics* **2013**, *32*, 127–136. [CrossRef]

51. Schwartz, M. *Innovations in Materials Manufacturing, Fabrication, and Environmental Safety*; CRC Press: Boca Raton, FL, USA, 2010; ISBN 9781420082166.

52. Parente, M.; Safdarian, R.; Santos, A.D.; Loureiro, A.; Vilaca, P.; Jorge, R.M.N. A study on the formability of aluminum tailor welded blanks produced by friction stir welding. *Int. J. Adv. Manuf. Technol.* **2016**, *83*, 2129–2141. [CrossRef]

53. Gullino, A.; Matteis, P.; D'Aiuto, F. Review of Aluminum-To-Steel Welding Technologies for Car-Body Applications. *Metals* **2019**, *9*, 315. [CrossRef]

54. Page, M.J.; McKenzie, J.E.; Bossuyt, P.M.; Boutron, I.; Hoffmann, T.C.; Mulrow, C.D.; Shamseer, L.; Tetzlaff, J.M.; Akl, E.A.; Brennan, S.E.; et al. The PRISMA 2020 statement: An updated guideline for reporting systematic reviews. *BMJ* **2021**. [CrossRef]

55. Xia, H.; Tan, C.; Tian, R.; Meng, S.; Li, L.; Ma, N. Influence of shielding gas on microstructure and mechanical properties of laser welded–brazed Al/steel lapped joint. *J. Manuf. Process.* **2020**, *54*, 347–358. [CrossRef]

56. Peyre, P.; Sierra, G.; Deschaux-Beaume, F.; Stuart, D.; Fras, G. Generation of aluminium–steel joints with laser-induced reactive wetting. *Mater. Sci. Eng. A* **2007**, *444*, 327–338. [CrossRef]

57. Zhao, H.; White, D.R.; DebRoy, T. Current issues and problems in laser welding of automotive aluminium alloys. *Int. Mater. Rev.* **1999**, *44*, 238–266. [CrossRef]

58. Zhang, P.; Shi, H.; Tian, Y.; Yu, Z.; Wu, D. Effect of zinc on the fracture behavior of galvanized steel/6061 aluminum alloy by laser brazing. *Weld. World* **2021**, *65*, 13–22. [CrossRef]

59. Weller, D.; Simon, J.; Stritt, P.; Weber, R.; Graf, T.; Bezençon, C.; Bassi, C. Temperature Controlled Laser Joining of Aluminum to Galvanized Steel. *Phys. Procedia* **2016**, *83*, 515–522. [CrossRef]

60. Huang, R.; Tan, C.; Sun, Y.; Gong, X.; Wu, L.; Chen, B.; Zhao, H.; Song, X. Influence of processing window on laser welding-brazing of Al to press-hardened 22MnB5 steel. *Opt. Laser Technol.* **2021**, *133*, 106566. [CrossRef]

61. Seffer, O.; Springer, A.; Kaierle, S. Investigations on remote laser beam welding of dissimilar joints of aluminum alloys and steel with varying sheet thicknesses for car body construction. *J. Laser Appl.* **2017**, *29*, 022414. [CrossRef]

62. Seffer, O.; Springer, A.; Kaierle, S. Investigations on remote laser beam welding of dissimilar joints of austenitic chromium-nickel steel (X5CrNi18-10) and aluminum alloy (AA6082-T6) for battery housings. *J. Laser Appl.* **2018**, *30*, 032404. [CrossRef]

63. Lahdo, R.; Springer, A.; Meier, O.; Kaierle, S.; Overmeyer, L. Investigations on laser welding of dissimilar joints of steel and aluminum using a high-power diode laser. *J. Laser Appl.* **2018**, *30*, 032422. [CrossRef]

64. Meco, S.; Pardal, G.; Ganguly, S.; Williams, S.; McPherson, N. Application of laser in seam welding of dissimilar steel to aluminium joints for thick structural components. *Opt. Lasers Eng.* **2015**, *67*, 22–30. [CrossRef]

65. Guan, Q.; Long, J.; Yu, P.; Jiang, S.; Huang, W.; Zhou, J. Effect of steel to aluminum laser welding parameters on mechanical properties of weld beads. *Opt. Laser Technol.* **2019**, *111*, 387–394. [CrossRef]

66. Fan, J.; Thomy, C.; Vollertsen, F. Effect of Thermal Cycle on the Formation of Intermetallic Compounds in Laser Welding of Aluminum-Steel Overlap Joints. *Phys. Procedia* **2011**, *12*, 134–141. [CrossRef]

67. Yan, S.; Hong, Z.; Watanabe, T.; Jingguo, T. CW/PW dual-beam YAG laser welding of steel/aluminum alloy sheets. *Opt. Lasers Eng.* **2010**, *48*, 732–736. [CrossRef]

68. Cui, L.; Chen, B.; Chen, L.; He, D. Dual beam laser keyhole welding of steel/aluminum lapped joints. *J. Mater. Process. Technol.* **2018**, *256*, 87–97. [CrossRef]

69. Yuan, R.; Deng, S.; Cui, H.; Chen, Y.; Lu, F. Interface characterization and mechanical properties of dual beam laser welding-brazing Al/steel dissimilar metals. *J. Manuf. Process.* **2019**, *40*, 37–45. [CrossRef]

70. Su, J.; Yang, J.; Li, Y.; Yu, Z.; Chen, J.; Zhao, W.; Liu, H.; Tan, C. Microstructure and mechanical properties of laser fusion welded Al/steel joints using a Zn-based filler wire. *Opt. Laser Technol.* **2020**, *122*, 105882. [CrossRef]

71. Yang, B.; Zhao, H.; Wu, L.; Tan, C.; Xia, H.; Chen, B.; Song, X. Interfacial microstructure and mechanical properties of laser-welded 6061Al/AISI304 dissimilar lap joints via beam oscillation. *J. Mater. Res. Technol.* **2020**, *9*, 14630–14644. [CrossRef]

72. Indhu, R.; Tak, M.; Vijayaraghavan, L.; Soundarapandian, S. Microstructural evolution and its effect on joint strength during laser welding of dual phase steel to aluminium alloy. *J. Manuf. Process.* **2020**, *58*, 236–248. [CrossRef]

73. Torkamany, M.J.; Tahamtan, S.; Sabbaghzadeh, J. Dissimilar welding of carbon steel to 5754 aluminum alloy by Nd:YAG pulsed laser. *Mater. Des.* **2010**, *31*, 458–465. [CrossRef]

74. Pereira, A.B.; Cabrinha, A.; Rocha, F.; Marques, P.; Fernandes, F.A.O.; Alves de Sousa, R.J. Dissimilar metals laser welding between DP1000 steel and aluminum alloy 1050. *Metals* **2019**, *9*, 102. [CrossRef]

75. Liu, G.; Gao, X.; Peng, C.; Liu, X.; Huang, Y.; Zhang, Y.; You, D. Tensile resistance, microstructures of intermetallic compounds, and fracture modes of welded steel/aluminum joints produced using laser lap welding. *Trans. Nonferr. Met. Soc. China* **2020**, *30*, 2639–2649. [CrossRef]

76. Mathieu, A.; Pontevicci, S.; Viala, J.; Cicala, E.; Matteï, S.; Grevey, D. Laser brazing of a steel/aluminium assembly with hot filler wire (88% Al, 12% Si). *Mater. Sci. Eng. A* **2006**, *435–436*, 19–28. [CrossRef]

77. Mathieu, A.; Shabadi, R.; Deschamps, A.; Suery, M.; Matteï, S.; Grevey, D.; Cicala, E. Dissimilar material joining using laser (aluminum to steel using zinc-based filler wire). *Opt. Laser Technol.* **2007**, *39*, 652–661. [CrossRef]

78. Ogura, T.; Wakazono, R.; Yamashita, S.; Saida, K. Dissimilar laser brazing of aluminum alloy and galvannealed steel and defect control using interlayer. *Weld. World* **2020**, *64*, 697–706. [CrossRef]

79. Liu, D.; Wang, J.; Xu, M.; Jiao, H.; Tang, Y.; Li, D.; Zhao, L.; Han, S. Evaluation of dissimilar metal joining of aluminum alloy to stainless steel using the filler metals with a high-entropy design. *J. Manuf. Process.* **2020**, *58*, 500–509. [CrossRef]

80. Chen, R.; Wang, C.; Jiang, P.; Shao, X.; Zhao, Z.; Gao, Z.; Yue, C. Effect of axial magnetic field in the laser beam welding of stainless steel to aluminum alloy. *Mater. Des.* **2016**, *109*, 146–152. [CrossRef]

81. Yan, F.; Wang, X.; Chai, F.; Ma, H.; Tian, L.; Du, X.; Wang, C.; Wang, W. Improvement of microstructure and performance for steel/Al welds produced by magnetic field assisted laser welding. *Opt. Laser Technol.* **2019**, *113*, 164–170. [CrossRef]
82. Yan, F.; Zhang, K.; Yang, B.; Chen, Z.; Zhu, Z.; Wang, C. Interface characteristics and reaction mechanism of steel/Al welds produced by magnetic field assisted laser welding-brazing. *Opt. Laser Technol.* **2021**, *138*, 106843. [CrossRef]
83. Qin, G.; Ji, Y.; Ma, H.; Ao, Z. Effect of modified flux on MIG arc brazing-fusion welding of aluminum alloy to steel butt joint. *J. Mater. Process. Technol.* **2017**, *245*, 115–121. [CrossRef]
84. Sun, J.; Yan, Q.; Li, Z.; Huang, J. Effect of bevel angle on microstructure and mechanical property of Al/steel butt joint using laser welding-brazing method. *Mater. Des.* **2016**, *90*, 468–477. [CrossRef]
85. Li, L.; Xia, H.; Tan, C.; Ma, N. Effect of groove shape on laser welding-brazing Al to steel. *J. Mater. Process. Technol.* **2018**, *252*, 573–581. [CrossRef]
86. Li, L.; Xia, H.; Tan, C.; Ma, N. Influence of laser power on interfacial microstructure and mechanical properties of laser welded-brazed Al/steel dissimilar butted joint. *J. Manuf. Process.* **2018**, *32*, 160–174. [CrossRef]
87. Xia, H.; Zhao, X.; Tan, C.; Chen, B.; Song, X.; Li, L. Effect of Si content on the interfacial reactions in laser welded-brazed Al/steel dissimilar butted joint. *J. Mater. Process. Technol.* **2018**, *258*, 9–21. [CrossRef]
88. Tan, C.; Zang, C.; Xia, H.; Zhao, X.; Zhang, K.; Meng, S.; Chen, B.; Song, X.; Li, L. Influence of Al additions in Zn–based filler metals on laser welding–brazing of Al/steel. *J. Manuf. Process.* **2018**, *34*, 251–263. [CrossRef]
89. Wallerstein, D.; Lusquiños, F.; Comesaña, R.; del Val, J.; Riveiro, A.; Badaoui, A.; Pou, J. Dissimilar unbeveled butt joints of AA6061 to S235 structural steel by means of standard single beam fiber laser welding-brazing. *J. Mater. Process. Technol.* **2021**, *291*, 116994. [CrossRef]
90. Xia, H.; Tao, W.; Li, L.; Tan, C.; Zhang, K.; Ma, N. Effect of laser beam models on laser welding–brazing Al to steel. *Opt. Laser Technol.* **2020**, *122*, 105845. [CrossRef]
91. Wallerstein, D.; Vaamonde, E.; Prada, A.; Torres, E.A.; Urtiga Filho, S.L.; Santos, T.F.A. Influence of welding gases and filler metals on hybrid laser-GMAW and Laser-FCAW welds. *Proc. Inst. Mech. Eng. Part C J. Mech. Eng. Sci.* **2020**. [CrossRef]
92. Chen, S.S.; Li, S.; Li, Y.; Huang, J.; Chen, S.S.; Yang, J. Butt welding-brazing of steel to aluminum by hybrid laser-CMT. *J. Mater. Process. Technol.* **2019**, *272*, 163–169. [CrossRef]
93. Meng, Y.; Gong, M.; Zhang, S.; Zhang, Y.; Gao, M. Effects of oscillating laser offset on microstructure and properties of dissimilar Al/steel butt-joint. *Opt. Lasers Eng.* **2020**, *128*, 106037. [CrossRef]
94. Bao, Y.; Zhou, J.; Zhang, Y.; Xu, Y.; Liu, H. Microstructural and mechanical characteristics of direct laser welding 7075 super hard aluminum alloy/D6AC ultra-high strength alloy structural steel. *Mater. Lett.* **2021**, *287*, 129312. [CrossRef]
95. Rong, J.; Kang, Z.; Chen, S.; Yang, D.; Huang, J.; Yang, J. Growth kinetics and thickness prediction of interfacial intermetallic compounds between solid steel and molten aluminum based on thermophysical simulation in a few seconds. *Mater. Charact.* **2017**, *132*, 413–421. [CrossRef]
96. He, H.; Gou, W.; Wang, S.; Hou, Y.; Ma, C.; Mendez, P.F. Kinetics of intermetallic compound layers during initial period of reaction between mild steel and molten aluminum. *Int. J. Mater. Res.* **2019**, *110*, 194–201. [CrossRef]
97. Takata, N.; Nishimoto, M.; Kobayashi, S.; Takeyama, M. Morphology and formation of Fe–Al intermetallic layers on iron hot-dipped in Al–Mg–Si alloy melt. *Intermetallics* **2014**, *54*, 136–142. [CrossRef]
98. Cheng, W.-J.; Wang, C.-J. Effect of silicon on the formation of intermetallic phases in aluminide coating on mild steel. *Intermetallics* **2011**, *19*, 1455–1460. [CrossRef]
99. Yin, F.; Zhao, M.; Liu, Y.; Han, W.; Li, Z. Effect of Si on growth kinetics of intermetallic compounds during reaction between solid iron and molten aluminum. *Trans. Nonferr. Met. Soc. China* **2013**, *23*, 556–561. [CrossRef]
100. Zhang, W.; Sun, D.; Han, L.; Liu, D. Interfacial microstructure and mechanical property of resistance spot welded joint of high strength steel and aluminium alloy with 4047 AlSi12 interlayer. *Mater. Des.* **2014**, *57*, 186–194. [CrossRef]
101. Azimaee, H.; Sarfaraz, M.; Mirjalili, M.; Aminian, K. Effect of silicon and manganese on the kinetics and morphology of the intermetallic layer growth during hot-dip aluminizing. *Surf. Coat. Technol.* **2019**, *357*, 483–496. [CrossRef]
102. Springer, H.; Kostka, A.; Payton, E.J.; Raabe, D.; Kaysser-Pyzalla, A.; Eggeler, G. On the formation and growth of intermetallic phases during interdiffusion between low-carbon steel and aluminum alloys. *Acta Mater.* **2011**, *59*, 1586–1600. [CrossRef]
103. Lemmens, B.; Springer, H.; De Graeve, I.; De Strycker, J.; Raabe, D.; Verbeken, K. Effect of silicon on the microstructure and growth kinetics of intermetallic phases formed during hot-dip aluminizing of ferritic steel. *Surf. Coat. Technol.* **2017**, *319*, 104–109. [CrossRef]
104. Ashby, M.F.; Easterling, K.E. The transformation hardening of steel surfaces by laser beams—I. Hypo-eutectoid steels. *Acta Metall.* **1984**, *32*, 1935–1948. [CrossRef]
105. Ion, J.C. (Ed.) Laser processing diagrams. In *Laser Processing of Engineering Materials*; Elsevier: Amsterdam, The Netherlands, 2005; pp. 178–187. ISBN 9780750660792.
106. Suder, W.J.; Williams, S.W. Investigation of the effects of basic laser material interaction parameters in laser welding. *J. Laser Appl.* **2012**, *24*, 032009. [CrossRef]
107. Suder, W.J.; Williams, S. Power factor model for selection of welding parameters in CW laser welding. *Opt. Laser Technol.* **2014**, *56*, 223–229. [CrossRef]

108. Van Alboom, A.; Lemmens, B.; Breitbach, B.; De Grave, E.; Cottenier, S.; Verbeken, K. Multi-method identification and characterization of the intermetallic surface layers of hot-dip Al-coated steel: FeAl$_3$ or Fe$_4$Al$_{13}$ and Fe$_2$Al$_5$ or Fe$_2$Al$_{5+x}$. *Surf. Coat. Technol.* **2017**, *324*, 419–428. [CrossRef]

109. You, D.Y.; Gao, X.D.; Katayama, S. Review of laser welding monitoring. *Sci. Technol. Weld. Join.* **2014**, *19*, 181–201. [CrossRef]

110. Dal, M.; Fabbro, R. An overview of the state of art in laser welding simulation. *Opt. Laser Technol.* **2015**, *78*, 1–13. [CrossRef]

111. Zhang, G.; Chen, M.; Shi, Y.; Huang, J.; Yang, F. Analysis and modeling of the growth of intermetallic compounds in aluminum–steel joints. *RSC Adv.* **2017**, *7*, 37797–37805. [CrossRef]

112. Yang, T.; Dai, W.; Zhuang, Y.; Liu, J.; Zhou, Z.; Hu, J. Investigation on the control of interfacial layer uniformity in laser-metal inert-gas hybrid welded-brazed Al/steel butt joint. *J. Manuf. Process.* **2020**, *58*, 1241–1250. [CrossRef]

113. Evdokimov, A.; Doynov, N.; Ossenbrink, R.; Obrosov, A.; Weiß, S.; Michailov, V. Thermomechanical laser welding simulation of dissimilar steel-aluminum overlap joints. *Int. J. Mech. Sci.* **2021**, *190*, 106019. [CrossRef]